Chemical Science

ROYAL SOCIETY OF CHEMISTRY

REVIEW

View Article Online
View Journal | View Issue

Cite this: *Chem. Sci.*, 2026, **17**, 3936

Positioning versatile inorganic cathode materials in the aqueous zinc-ion battery landscape

Kang Guo,[a] Yaokang Lv,[d] Ziyang Song,[*ab] Lihua Gan[*ac] and Mingxian Liu[*ac]

Rechargeable aqueous zinc-ion batteries (AZIBs) have attracted great attention due to their inherent advantages such as high safety, low cost, and environmental friendliness, making them one of the most promising alternatives to traditional lithium-ion batteries. The rational design and continuous optimization of versatile inorganic cathode materials play a crucial role in achieving practical applications. In this review, we first systematically classify inorganic cathode materials and their design strategies, including manganese oxides with rich redox chemistry, vanadium compounds with multiple oxidation states, Prussian blue analogues with open skeleton channels, layered transition metal disulfides with unique interlayer ion storage capabilities, and halogens with reversible multielectron capacity. Furthermore, the structural characteristics, electrochemical performances, and crucial improvement methods of these cathode materials are discussed in detail. Finally, we outline the challenges and the prospects of inorganic cathodes in AZIBs to guide the future development of next-generation energy communities.

Received 5th December 2025
Accepted 31st January 2026

DOI: 10.1039/d5sc09531j

rsc.li/chemical-science

[a]*Shanghai Key Lab of Chemical Assessment and Sustainability, School of Chemical Science and Engineering, Tongji University, 1239 Siping Rd., Shanghai, 200092, P. R. China. E-mail: ganlh@tongji.edu.cn; liumx@tongji.edu.cn*

[b]*State Key Laboratory of Pollution Control and Resource Reuse, College of Environmental Science and Engineering, Advanced Research Institute, Tongji University, 1239 Siping Rd., Shanghai, 200092, P. R. China. E-mail: songziyang@tongji.edu.cn*

[c]*State Key Laboratory of Cardiovascular Diseases and Medical Innovation Center, Shanghai East Hospital, School of Medicine, Tongji University, 150 Jimo Rd., Shanghai, 200120, P. R. China*

[d]*College of Chemical Engineering, Zhejiang University of Technology, 18 Chaowang Rd., Hangzhou 310014, P. R. China*

Kang Guo

Kang Guo is currently a PhD student at School of Chemical Science and Engineering in Tongji University under the supervision of Professor Mingxian Liu. He received his master's degree (2022) from Shanghai Electric Power University. His research interests focus on the structural design and functional modulation of inorganic materials in aqueous batteries.

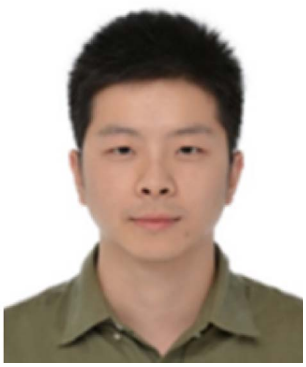

Ziyang Song

Ziyang Song received his PhD degree from School of Chemical Science and Engineering in Tongji University (2021). He started his postdoctoral researches at Tongji University (2021–2025). After that, he joined College of Environmental Science and Engineering in Tongji University, and became a specially appointed researcher in 2025. His research interest focuses on the structural design of redox-active aromatic organic materials and self-assembled nanostructured carbon materials towards electrochemical energy storage applications involving versatile aqueous batteries and capacitors.

1. Introduction

With the rapid progress of modern technologies, the extensive use of portable electronics and electric vehicles has intensified the demand for efficient storage systems capable of accommodating fluctuating and intermittent renewable energy, highlighting the necessity for high energy density devices.[1–6] Lithium-ion batteries have established themselves as the cornerstone of modern rechargeable energy storage, owing to their high energy density and exceptional cycle stability.[7,8] Yet, concerns over safety stemming from flammable organic electrolytes alongside environmental impact, volatile pricing, and constrained supply of critical metals such as lithium and cobalt, have cast growing doubt on their long-term viability.[9–11] These limitations have spurred increasing interest in alternative chemistries based on earth-abundant elements such as sodium and potassium.[12–17] While resource accessibility is a clear advantage, the large ionic radii and high reactivity of these species impose significant challenges in identifying stable and efficient electrode materials. Aqueous electrolyte systems, by contrast, offer a compelling path forward, combining high ionic conductivity, intrinsic safety, and low cost positioning them as promising candidates for next-generation sustainable energy storage.[18–27]

Among aqueous-based energy storage systems, aqueous zinc-ion batteries (AZIBs) have garnered significant interest due to several inherent advantages:[28–33] (1) a low redox potential of Zn/Zn^{2+}, suitable for both neutral and mildly acidic media (-0.76 V *vs.* standard hydrogen electrode, SHE), and even lower in alkaline environments; (2) high theoretical specific capacity and exceptional volumetric capacity; (3) aqueous electrolytes have higher ionic conductivity; (4) they are non-flammable, environmentally benign, and compatible with ambient-air assembly benefiting from the richness and stability of metallic zinc. These merits make AZIBs promising for safe, low-cost applications. However, their energy density remains suboptimal compared to organic electrolyte-based systems.[34–36] Challenges such as the narrow electrochemical stability window of water, limited discharge capacity, parasitic side reactions, and relatively low output voltage significantly constrain their practical performance.[37–39] In response, intensive research efforts have been directed toward enhancing the capacity and energy density of aqueous AZIBs through materials innovation and system-level design.

The practical implementation of AZIBs is hindered by the scarcity of inorganic cathode materials capable of meeting multiple critical requirements simultaneously.[40–42] To date, different inorganic cathode materials have been explored in AZIBs, which show versatile advantages of broad structure–function tunability (*i.e.*, heteroatom doping, lattice defects, interlayer extension, interface heterojunction engineering), different charge storage mechanisms of Zn^{2+}/H^{+} insertion/extraction and halogen multivalent conversion; (iii) board-range performance optimization (capacity, rate capability, energy density, and life) in aqueous conditions. These requirements encompass sufficient structural adaptability to accommodate the strong electrostatic interactions of divalent Zn^{2+} ions, high specific capacity, appropriate and stable operating voltage, robust cycling stability, as well as environmental friendliness and economic feasibility. The electrochemical and economic advantages of aqueous zinc ion batteries largely depend on the inherent properties of the inorganic cathode materials used.[43] Specifically, the rate performance is strongly governed by the ion and electron transport kinetics, together with the interfacial reaction behavior between the electrode and the electrolyte, while the cycle life is largely dependent on the structural integrity and stability of the electrode framework during repeated (dis)charge processes.[44–46] Thus, the rational engineering and optimization of versatile inorganic cathode materials that simultaneously deliver high capacity, structural robustness, and sustainability represent a key strategy to overcome current limitations and to accelerate the practical application and industrialization of AZIBs technology.

As shown in Fig. 1, the historical development of AZIBs cathode materials have undergone continuous evolution, reflecting extensive efforts to improve their electrochemical performance and structural stability. So far, various strategies

Lihua Gan

Lihua Gan received his PhD degree in materials physics and chemistry in Tongji University, and became a professor in Department of Chemistry, Tongji University (2005). His research interests include the design and application of nanomaterials, which cover porous metal oxides, various carbonaceous materials and carbon-based materials. These nanomaterials are used for adsorbents, supercapacitors, and batteries.

Mingxian Liu

Mingxian Liu received his PhD degree in physical chemistry in Tongji University (2009). He started his postdoctoral researches in East China University of Science and Technology (2009–2011). After that, he joined School of Chemical Science and Engineering in Tongji University, and became a professor in 2016. His current research interests focus on the structural design of electrode materials for electrochemical storage including carbon-based supercapacitors, zinc-ion hybrid supercapacitors, and zinc-ion batteries.

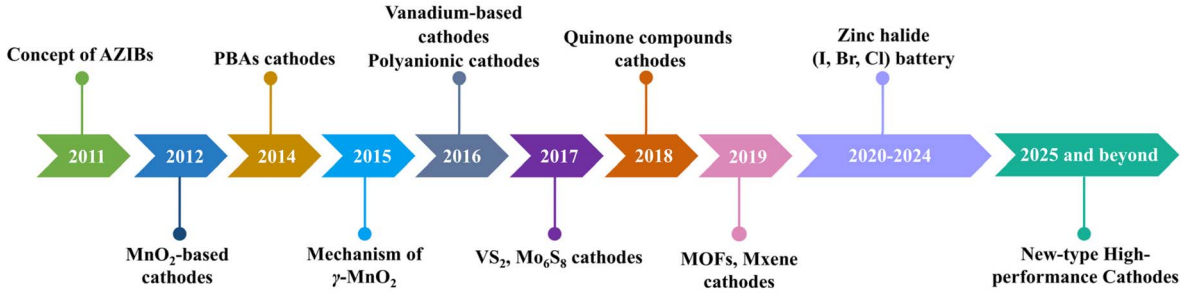

Fig. 1 Timeline of the historical development of inorganic cathode materials for AZIBs.

for designing high-performance versatile cathodes have been explored, including manganese (Mn)-based compounds with rich redox activity, vanadium(V)-based materials with multiple oxidation states, Prussian blue analogues (PBAs) with open framework channels, layered transition metal sulfides with unique interlayer ion storage capabilities, and multi electron reversible, high-capacity halogen cathode materials. These systems not only showcase the diversity of material chemistry, but also highlight the challenges of achieving high capacity, long-term cycling stability, and fast ion transport simultaneously. Thus, this review emphasizes the latest advances of different inorganic cathode materials in controlled synthesis, potential electrochemical mechanisms, and rational design strategies (Fig. 2). By consolidating these advances, we aim to provide comprehensive analysis and direction for the rational design of next-generation inorganic cathode materials, ultimately accelerating the practical application of high-performance AZIBs in large-scale energy storage systems.

2 Mn-based cathodes

Manganese-based compounds are recognized as prospective versatile inorganic cathode candidates for AZIBs owing to the abundant redox chemistry and resource availability.[47–50] Manganese is widely distributed in the Earth's crust, predominantly in the form of oxide ores, providing a solid material basis for large-scale deployment in energy storage. These compounds can undergo multiple valence transitions (*e.g.*, Mn^{4+}/Mn^{3+} and Mn^{4+}/Mn^{2+}), often accompanied by single- or two-electron transfer processes, which endow them with high capacity and considerable energy output. Moreover, manganese oxides typically feature high operating voltages and favorable theoretical capacities, further underscoring their potential as attractive inorganic cathode systems. To this end, various crystalline frameworks have been explored, ranging from different polymorphs of MnO_2 to spinel-type $ZnMn_2O_4$.[51–54]

Despite these advantages, several challenges hinder their practical implementation. Although its ionic radius is comparable to lithium, Zn^{2+} exhibits strong coulomb interactions with the electrode skeleton, which severely limits diffusion and slows down the intercalation process. In the absence of rational structural engineering, it is difficult to realize efficient and reversible Zn^{2+} storage. In addition, the inherently low electrical conductivity and sluggish ion transport of manganese oxides further restrict their rate capability. Compounding these issues, long-term cycling often triggers structural distortions, Mn dissolution, and active component depletion, ultimately result in severe capacity fading and limited battery lifespan.[55–57]

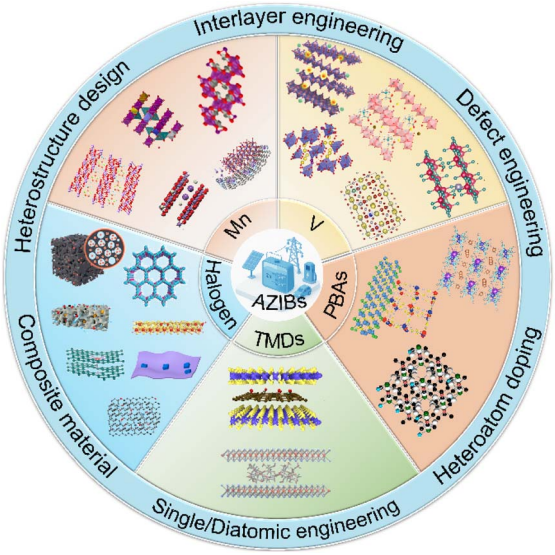

Fig. 2 Schematic diagram of different inorganic cathode materials and design strategies.

2.1 MnO_2 materials

The porous skeleton (tunnel/layered configuration) of MnO_2 can stably support reversible insertion/deintercalation of Zn^{2+}, making it the preferred Mn-based versatile inorganic cathode material for AZIBs.[58–62] However, the delayed ion migration kinetics, insufficient intrinsic conductivity, and manganese leaching effect still constrain its performance improvement.[63–65] In recent years, researchers have been continuously advancing the practical application of MnO_2 lattice and interface composition in AZIBs to enhance cycling stability.[66–68]

Research has shown that doping with non-metallic heteroatoms can effectively regulate the electronic structure and surface chemistry of MnO_2, improve conductivity and ion diffusion channels, thereby enhancing its specific capacity and cycling stability. Liu team enhanced the cycling stability of MnO_2 by doping nitrogen and sulfur into MnO_2 (NS-MnO_2) through a simple annealing strategy (Fig. 3a).[69] Research shows that N/S co-doping establishes Mn–N and Mn–S bonds within

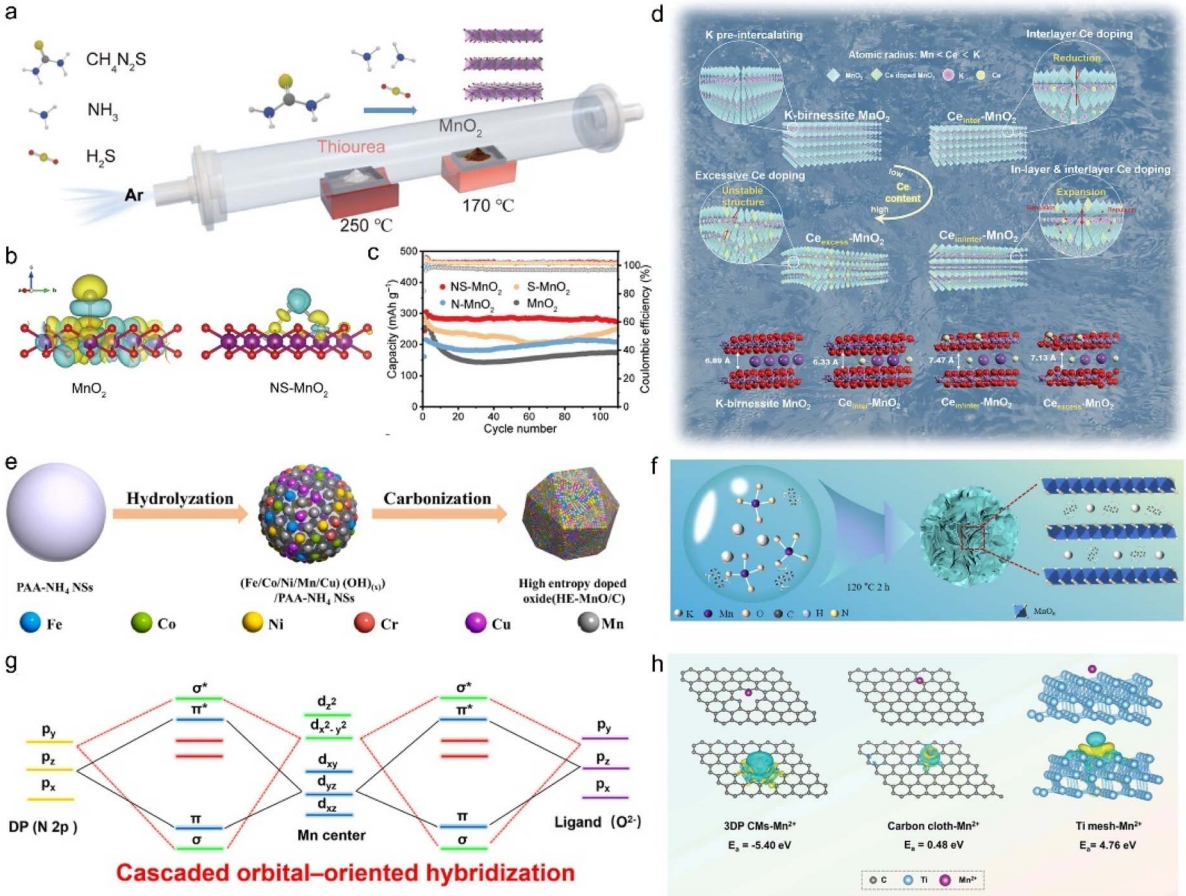

Fig. 3 Multiscale structural engineering of MnO_2. (a) Synthesis process, (b) charge density difference distribution, and (c) cycling performance of the NS-MnO_2 material.[69] Copyright 2025, Wiley-VCH. (d) Schematic birnessite structures and Density functional theory (DFT) calculated structures of pristine δ-MnO_2 (K-birnessite MnO_2) and Ce doped δ-MnO_2 (Ce_{inter}-MnO_2, $Ce_{in/inter}$-MnO_2, Ce_{excess}-MnO_2).[70] Copyright 2023, Wiley-VCH. (e) Synthesis schematic of HE-MnO/C.[72] Copyright 2024, Elsevier. (f) Schematic illustration of the NAPD pre-intercalation process.[73] Copyright 2024, Elsevier. (g) Schematic illustration of the cascaded orbital-oriented hybridization mechanism.[74] Copyright 2022, Wiley-VCH (h) adsorbing energy and charge difference density simulations of Mn^{2+} on the surface of the 3DP CMs, carbon cloth, and Ti mesh.[75] Copyright 2022, Wiley-VCH.

the lattice. The Mn–N configuration suppresses Jahn–Teller distortion in Mn^{3+} species, while Mn–S bonding reduces Zn^{2+}-cathode electrostatic interactions, enabling reversible Mn^{4+}/Mn^{3+} redox without by-product formation (Fig. 3b). This co-doping strategy simultaneously elevates intrinsic conductivity, significantly accelerating reaction kinetics. Benefitting from these synergistic effects, the NS-MnO_2 cathode delivers exceptional electrochemical performance, outstanding cycling durability (295 mAh g^{-1} at 0.2 A g^{-1}) and maintains structural stability (1500 cycles at 1 A g^{-1}, Fig. 3c).

Compared with non-metallic heteroatom doping, metal ion doping can significantly improve the zinc storage capacity and cycle life of MnO_2 by adjusting the lattice structure and valence state distribution, expanding the interlayer spacing, enhancing structural stability, and introducing more reversible redox sites. Xu group developed Ce-doped δ-MnO_2 as a high-performance AZIBs inorganic cathode and investigated the effects of different doping positions (Fig. 3d).[70] At low Ce content, cations occupy interlayer sites (Ce_{inter}-MnO_2), while higher doping introduces Ce into both interlayer and lattice positions ($Ce_{in/inter}$-MnO_2), forming alternating layered structures. Excessive doping may trigger phase transitions (Ce_{excess}-MnO_2). $Ce_{in/inter}$-MnO_2 notably enlarges the interlayer spacing, providing more zinc storage sites and faster ion diffusion. Ce doping also generates oxygen vacancies and loosens the flower-like structure, enhancing conductivity and increasing electrochemical active sites. As a result, $Ce_{in/inter}$-MnO_2 delivers a maximum capacity of 393.0 mAh g^{-1} at 300 mA g^{-1} and maintains 148.9 mAh g^{-1} after 2000 cycles at 3 A g^{-1} with nearly 100% retention.

Zhao *et al.*[71] mitigated the conflict between electrochemical kinetics and durability in AZIBs by developing Al-doped, defect-rich MnO_2 nanosheets (Al_x–MnO_2) *via* electrochemical oxidation of MnAl-LDHs. Al^{3+} vacancies served as 3D Zn^{2+} diffusion channels, while residual Al suppressed lattice distortion, preserving structural integrity. The modified $Al_{0.1}$–MnO_2 showed high capacity, fast kinetics, and longer cycle life, exceeding most of the current Mn- and V-based versatile inorganic cathodes. Compared to a single metal, the doping effect of multiple high entropy materials is more pronounced. Wang

et al.[72] introduced multiple metal dopants into a single oxide matrix and formed high entropy HE-MnO/C composites through *in situ* confinement, achieving a robust cathode for AZIBs (Fig. 3e). The dopants selected for ionic radius compatibility and electrochemical function, enhanced voltage (Cr, Cu), structural stability (Co, Zn), and redox activity (Ni). Compared to single doping, entropy-driven stabilization suppressed Mn dissolution, as supported by theoretical insights showing stronger Mn–O bonding. Defect-induced kinetics further improved durability (after 10 000 cycles at 10 A g^{-1}, the capacity retention rate was 93.2%). This study highlights the promise of high-entropy materials for advanced AZIBs versatile inorganic cathodes.

In addition to inserting metal ions into the interlayer, the insertion of organic materials is also very effective in enhancing the framework stability, charge storage capability, and conductivity of Mn-based oxides. Huang *et al.*[73] designed a hybrid cathode by pre-intercalating 1,5-diaminonaphthalene (NAPD) into potassium manganese oxide (KMO), yielding KMO-NAPD with enhanced electrochemical performance (Fig. 3f). The incorporation of NAPD modulated the d-electron spin states of Mn, boosting Zn^{2+} intercalation activity and reducing Zn^{2+}–host interaction through weakened electrostatic forces, thereby facilitating ion diffusion. So that, the assembled AZIBs also exhibited an impressive energy density of 294.3 Wh kg^{-1} alongside a maximum power output of 8.6 kW kg^{-1}. Yang *et al.*[74] proposed a cascaded orbital-oriented hybridization strategy by introducing 1,3-propanediamine (DP) to construct an organic–inorganic hybrid framework. The P_x and P_z orbitals of the nitrogen atoms in DP engage in antibonding σ-hybridization with Mn $d_{x^2-y^2}$ orbitals near the Fermi level, thereby elevating the energy of Mn $d_{x^2-y^2}$ state and enabling its further hybridization with O P_y orbitals in the MnO_2 lattice (Fig. 3g). This orbital reconstruction selectively accelerates proton-storage kinetics while exerting a negligible effect on the Zn^{2+} insertion pathway. Consequently, the resulting DP-MnO_2 composite exhibits outstanding rate capability and long-term cycling stability.

Repeated ion insertion/extraction of MnO_2 can easily lead to crystal structure collapse and pulverization, causing contact failure between the active substance and the current collector, resulting in rapid capacity decay. Introducing carbon materials to form composite structures has become an effective strategy to overcome these bottlenecks. Yang *et al.*[75] abdicated 3D-printed carbon microlattices (3DP CMs) using graphene and carbon nanotubes *via* direct ink printing followed by high-temperature annealing (Fig. 3h). The printing enabled periodic architectures, while annealing enhanced conductivity and introduced surface defects. These features promoted uniform electric field distribution and enhance the controlled growth of MnO_2. Notably, 3DP CM electrode incorporating MnO_2 delivered an unprecedented specific capacity of 282.8 mAh g^{-1} (mass loading: 28.4 mg cm^{-2}) and, offering an effective route toward designing advanced AZIBs electrodes. Fan *et al.*[76] designed CNT-MnO_2 (C-MnO_2) nanorods using carbonylated CNTs as a "defense shield" to promote proton insertion and ensure stable, fast-charging Zn–Mn batteries. The CNT network shortened ion diffusion paths and offered abundant proton sites, enhancing charge transport and structural reversibility. Meanwhile, carboxyl groups and Mn–O–C bonds suppressed Mn^{2+} dissolution and improved redox stability. Therefore, C-MnO_2 cathode has achieved high capacity and excellent cycling performance. In order to ensure sustainable material sources, low costs, and environmental friendliness, Lv *et al.*[77] successfully prepared γ-MnO_2 uniformly loaded on nitrogen doped carbon in grapefruit peel using biomass materials (γ-MnO_2@CP). After 3000 cycles under the condition of 5 A g^{-1}, the capacity retention rate reached as high as 92.17%.

MnO_2-based cathodes face critical limitations, including poor electronic conductivity, structural collapse during cycling, active material dissolution, and sluggish Zn^{2+} diffusion. Recent advances have introduced several targeted strategies to mitigate these issues.[78,79] First, elemental doping and defect modulation effectively reshape the electronic environment and surface reactivity, thereby enhancing charge transport, stabilizing redox reactions, and preventing irreversible phase changes. Second, interlayer engineering *via* the pre-intercalation of guest species into layered MnO_2 helps maintain interplanar spacing, promoting ion diffusion and structural reversibility. Third, compositing with carbon-based frameworks improves conductivity and mechanical resilience, while also increasing surface area and exposing more active sites. These multifaceted strategies pave the way for next-generation, high-efficiency MnO_2 versatile inorganic cathodes in AZIBs systems.

2.2 Other Mn-based materials

In addition to MnO_2, other Mn-based oxides such as Mn_3O_4, MnO, and spinel-type compounds (*e.g.*, $M_xMn_2O_4$, where M = Zn, Mg, *etc.*) have also been explored as versatile inorganic cathode materials for AZIBs.[80–82] These materials exhibit distinct energy storage mechanisms: Mn_3O_4 and Mn_2O_3 typically undergo multivalent redox reactions involving Mn^{3+}/Mn^{2+} or Mn^{4+}/Mn^{3+} transitions during Zn^{2+} intercalation or phase transformation. MnO, with a simpler cubic structure and lower valence state, stores charge primarily through reversible redox conversion reactions. Spinel-type $M_xMn_2O_4$ compounds, where Zn^{2+} or other metal ions are pre-intercalated into the lattice, enable structural stabilization during Zn^{2+} reinsertion and reversible Mn redox processes. Despite their structural diversity, these Mn-based oxides often suffer from rapid capacity fading, manganese dissolution, poor intrinsic electronic conductivity, and sluggish Zn^{2+} diffusion, all of which limit their long-term cycling stability and rate capability.

Manganese dissolution is one of the key issues leading to a decrease in the cycling stability of Mn-based oxide cathode materials, such as Mn_3O_4. The limited redox kinetics and sustained manganese dissolution jointly lead to low activity, rapid capacity decay, and shortened cycle life of Mn_3O_4 electrode. For this, Deng *et al.*[83] proposed a novel strategy combining vanadium vacancy engineering with Mn-ion confinement, yielding a composite cathode denoted as VMn-Mn_3O_4@C (Fig. 4a–c). The introduction of cationic V vacancies created additional active site significantly enhancing capacity. Simultaneously, the

carbon matrix restricted Mn ion migration, effectively suppressing dissolution and improving structural durability. Thus, Zn/VMn-Mn_3O_4@C cell achieved a performance of 280.9 mAh g^{-1} at a low current of 0.1 A g^{-1} and ion diffusion coefficient. More notably, the capacity remained nearly unchanged after 5000 cycles at 1 A g^{-1}, offering a promising pathway for designing high-performance Mn-based cathodes in AZIBs.

Tailoring reversible and robust crystal structures in Mn-based materials remains a critical yet challenging task. To this end, Liu group developed a controllable electrochemical oxidation-induced phase transformation strategy, enabling the conversion of cubic α-Mn_2O_3 into an amorphous $Zn_{0.17}$-$MnO_{2-n}\cdot 0.52H_2O$ (Fig. 4d–f).[84] This amorphous phase, serving as the active Zn^{2+} host, offers abundant and accessible Zn-affinitive sites while alleviating lattice strain during Zn^{2+} (de) intercalation (Fig. 4g). Structural evolution analyses and theoretical simulations confirm that this amorphous phase exhibits excellent electronic conductivity and low Zn^{2+} migration barriers, and can reversibly transform into crystalline $ZnMn_3O_7\cdot 3H_2O$ during cycling. The stabilized dynamic transformation equilibrium underpins a remarkable specific capacity of 558 mAh g^{-1}, a high energy density of 696 Wh kg^{-1} at 6 kW kg^{-1}, and exceptional long-term cycling stability over 5000 cycles. Moreover, this strategy is extendable to other Mn-based systems such as Mn_3O_4 and α-MnO_2, offering new insights into electrochemical oxidation-driven crystal engineering for highly reversible and durable AZIBs.

MnO suffers from limited redox activity due to its stable Mn^{2+} state and lacks Mn^{3+}/Mn^{4+} conversion. Its poor conductivity and sluggish Zn^{2+} diffusion further restrict rate capability. To overcome these drawbacks, Li *et al.*[85] synthesized a composite cathode materia by embedding ultrafine VN quantum dots and MnO nanoparticles in a nitrogen-doped carbon matrix (NC@VN/MnO) *via in situ* self-polymerization (Fig. 4h). The VN-MnO heterostructure induces interfacial polarization and a built-in electric field, enhancing ion/electron transport and structural stability. So that, the cathode delivers 108.3 mAh g^{-1} after 12 000 cycles at 10 A g^{-1}, showing outstanding durability and electrochemical performance.

In AZIBs, protons actively contribute throughout the entire energy storage process. Nevertheless, the proton transport mechanism in metal oxide cathodes remains highly debated, largely due to the lack of suitable model systems, particularly with respect to how cation distribution modulates proton-conducting pathways. Using spinel-type $ZnMn_2O_4$ as a prototype, Pan and co-workers demonstrated that reducing the Zn content in the lattice by half nearly doubled the high-rate capacity, primarily owing to enhanced proton storage (Fig. 4i).[86] Detailed analysis revealed that in Zn-deficient structures, protons migrate efficiently through cooperative transport, whereas in stoichiometric counterparts, proton insertion follows a much slower and sequential process. Moreover, the intrinsically restricted Zn mobility within the spinel framework confers strong structural stability, preventing external Zn^{2+} from occupying Zn vacancies during cycling and thereby preserving proton storage advantages. These findings highlight that tailoring non-stoichiometric features represents a promising strategy to optimize proton conduction and storage performance in aqueous batteries.

The modification for MnO_2 targets their main issues of poor electronic transport, slow ion diffusion, and structural instability during interfacial electrochemical reactions in AZIBs: (i)

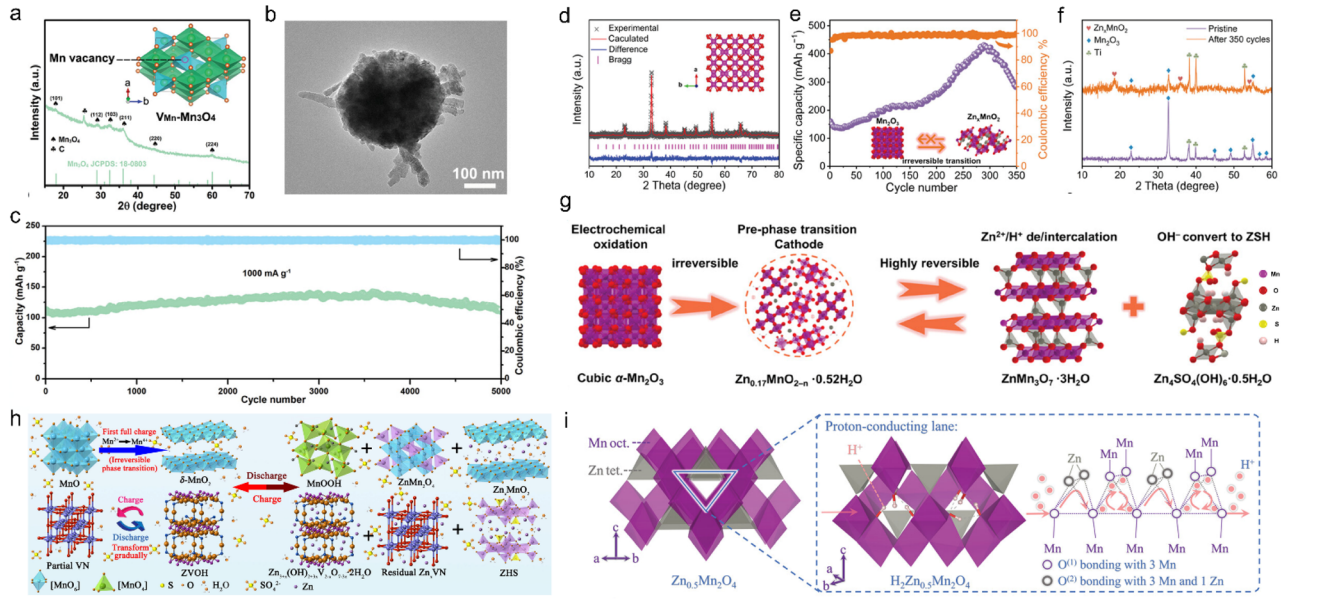

Fig. 4 Phase change engineering in Mn-based cathodes. (a) XRD pattern, (b) TEM image, and (c) long-term cycling performance of VMn-Mn_3O_4@C.[83] Copyright 2024, Wiley-VCH. (d) XRD pattern, (e) cycling performance, and (f) XRD patterns before and after cycling of α-Mn_2O_3. (g) Schematic diagram of the electrochemical reaction process of the $Zn_{0.17}MnO_2\cdot 0.52H_2O$ cathode.[84] Copyright 2024, Wiley-VCH. (h) Schematic illustration of phase transition mechanism.[85] Copyright 2023, Elsevier. (i) Theoretical calculations of proton intercalation in $Zn_{0.5}Mn_2O_4$.[86] Copyright 2022, Wiley-VCH.

regarding the poor electronic transport of MnO_2 cathodes (*e.g.*, high polarization, charge-transfer resistance and severe rate decay), mixing MnO_2 with highly conductive skeletons (carbon and polymers) is efficient to build continuous conductive networks for enhancing electron percolation and accelerating reaction kinetics towards efficient charge storage; (ii) to alleviate the problem of slow ion diffusion within MnO_2 host (*e.g.*, low GITT diffusion coefficient and low capacity contribution), it is beneficial to design Mn/O vacancies, expand Mn–O interlayers, or construct p–n heterojunctions (*e.g.*, MnO_2/MoS_2 hybrid), which provide desirable platforms to optimize Zn^{2+} diffusion channels and surface wettability with low energy barriers; (iii) to avoid the structural change and dissolution (*e.g.*, Mn dissolution, collapse, irreversible phase evolution), lattice-stabilized metal-ion doping is preferred to strengthen Mn–O bonding and suppress Jahn–Teller distortions/phase transitions. It should be pointed out that each strategy has boundary conditions and usage standards, and the most suitable regulatory strategy should be selected based on the target indicators.

In summary, Mn-based oxides, particularly MnO_2, have shown great potential as versatile inorganic cathodes for AZIBs owing to their open frameworks and rich redox chemistry, but their practical performance is still restricted by poor intrinsic conductivity, sluggish Zn^{2+} diffusion, structural collapse, and Mn dissolution.[87] Recent studies have demonstrated that elemental doping/defect modulation, interlayer engineering (*via* guest species pre-intercalation), and compositing with conductive carbon frameworks can effectively reshape the electronic environment, stabilize the host structure, and accelerate ion/electron transport, thereby improving capacity, rate capability, and cycling stability. Other Mn-based oxides such as Mn_3O_4, Mn_2O_3, MnO, and spinel-type $M_xMn_2O_4$ also benefit from defect, phase, and interface engineering to construct more reversible and robust Zn^{2+}/H^+ storage hosts.

Despite this progress, significant challenges remain, including capacity degradation under practical mass loading, competitive Zn^{2+}/H^+ reactions, and insufficient understanding of dissolution and phase evolution. Future research should therefore focus on: (i) designing precisely doped and defect-regulated Mn-based lattices, including high-entropy and non-stoichiometric systems, to simultaneously optimize electronic structure, ion transport, and Mn stability; (ii) constructing interlayer-engineered and organic–inorganic hybrid frameworks that decouple and co-optimize Zn^{2+} and proton storage while maintaining structural integrity under long-term operation; (iii) developing multidimensional conductive architectures and biomass-derived carbon scaffolds to realize thick, flexible, and mechanically robust Mn-based cathodes with high areal capacity; and (iv) integrating advanced *in situ*/*operando* characterizations with multiscale simulations to elucidate redox mechanisms and transport pathways, thereby guiding rational material design. Additionally, by embedding Mn-based oxides into printable, self-supporting carbon frameworks, binder-free and potentially biocompatible electrodes can be constructed, which may be extended to flexible and implantable AZIBs, further broadening the application landscape of Mn-based versatile inorganic cathodes.

3 V-based cathodes

Vanadium based compounds have become another versatile inorganic cathode material for AZIBs due to their multivalent properties (from V^{2+} to V^{5+}), adjustable crystal structure (including layering, tunneling, 3D framework, *etc.*), high theoretical capacity, fast reaction kinetics, and excellent cycle life at high current densities.[88] Due to its uniqueness, AZIBs has aroused great interest among people. To date, a wide array of vanadium-containing materials has been explored as cathodes, including vanadium oxides (layered or tunneled structures), vanadium nitrides, chalcogenides, V–C composites, and NASICON-type phases such as $Na_3V_2(PO_4)_3$.

3.1 V_2O_5-based materials

Layered V_2O_5 stands out as one of the most widely studied and structurally stable V-based oxides.[89–91] It offers a high theoretical capacity of 589 mAh g^{-1} and a favorable interlayer spacing of ~4.7 Å, which facilitates the diffusion of charge carriers.[92] Nevertheless, its practical application in aqueous electrolytes is limited by several factors, including a comparatively reduced working voltage (~0.8 V *vs.* Zn), sluggish ionic conductivity, and the tendency of vanadium to dissolve into the electrolyte.[93,94] To address such issues, various strategies have been introduced to enhance structural stability, redox kinetics, and electrochemical performance of materials.[95–97] Considering the rapid progress in this field, a timely and comprehensive review of recent advances in V_2O_5-based AZIBs is essential for providing insights into their underlying mechanisms and guiding future research directions.

Introducing cations (M^+) into the interlayer can increase the interlayer spacing, enhance structural stability, and promote the migration of Zn^{2+}. Notably, the type of inserted cation plays a critical role in modulating material properties. To this end, Hu *et al.*[89] developed a universal supramolecular self-assembly strategy to fabricate ultrathin $M_xV_2O_5$ nanosheets incorporating a wide range of single and multiple cations (Fig. 5a). Single-cation intercalation significantly enhanced Zn^{2+} diffusion kinetics and specific capacity, while multi-cation systems improved structural stability and cyclic reversibility *via* cooperative pillar effects. The optimized configuration exhibited a remarkable Zn^{2+} diffusion coefficient of 7.5×10^{-8} cm^2 s^{-1}, outperforming the majority of previously reported vanadium-derived cathode materials (Fig. 5b and c). This work presents a versatile multi-cation confinement strategy for advancing AZIBs inorganic cathodes and offers new insights into supramolecular guest-ion regulation of ion transport. To address the challenges associated with vanadium oxides, such as limited interlayer spacing, poor reversibility, and high solubility. Liu's group proposed an inorganic–organic co-intercalation strategy and successfully developed a layered cathode material, $[Al_{0.16}(C_5H_{14}ON)_{0.12}]V_2O_5 \cdot 0.39H_2O$ (IO-V_2O_5).[98] This hybrid system expands the interlayer distance to 13.7 Å and reinforces structural integrity, enabling enhanced performance in AZIBs

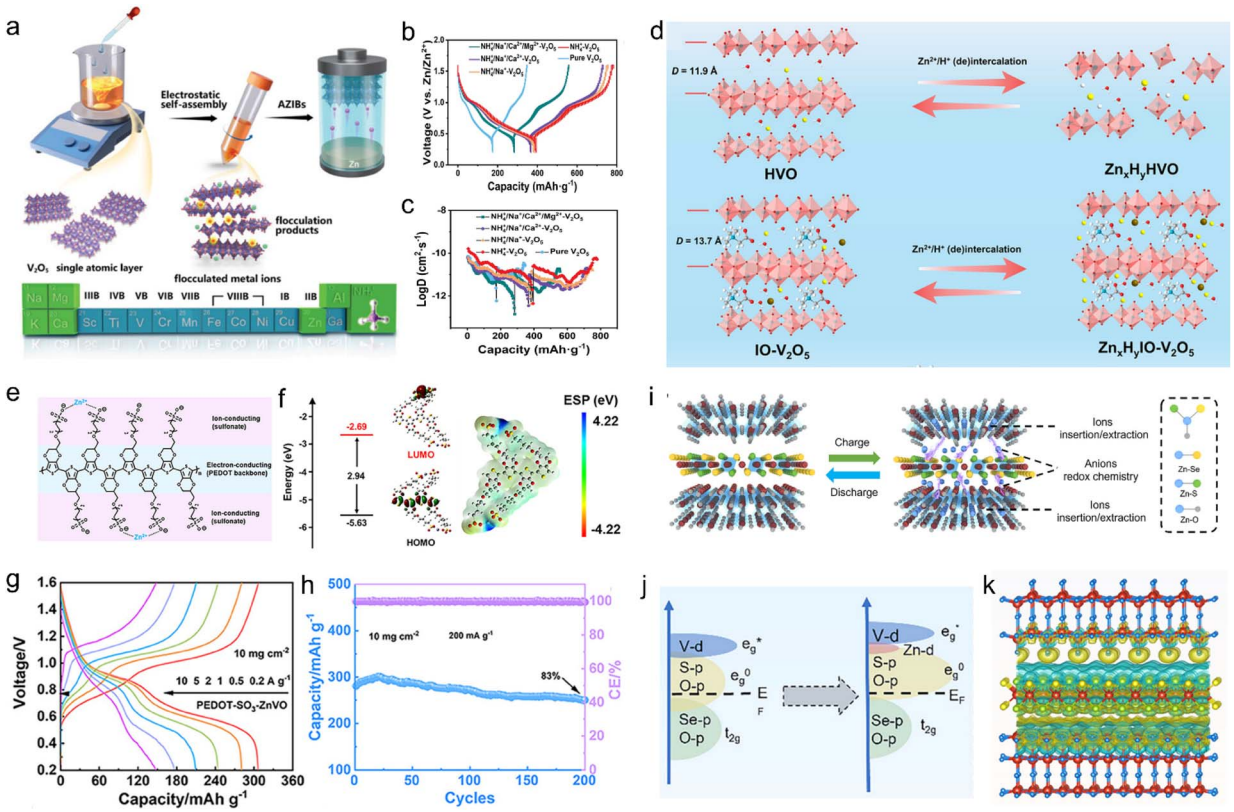

Fig. 5 Multi angle optimization strategy for V_2O_5 cathode. (a) Schematic supramolecular self-assembly strategy, and (b and c) analysis of ion diffusion coefficients for $M_xV_2O_5$.[89] Copyright 2023, Wiley-VCH. (d) Schematic mechanisms and structural advantages of IO-V_2O_5 cathode in AZIBs.[98] Copyright 2025, Wiley-VCH. (e) PTS conduction mechanism, (f) DFT calculations, and (g and h) electrochemical performance of PEDOT-SO_3-ZnVO.[99] Copyright 2024, Wiley-VCH. (i) Energy storage mechanism. (j) Schematic energy bands and its discharged state. (k) Charge density distribution.[100] Copyright 2024, Wiley-VCH.

(Fig. 5d). In this structure, Al^{3+} and betaine act as dual interlayer pillars, establishing rapid 2D Zn^{2+} transport channels. The quaternary ammonium group in betaine strongly interacts with the lattice oxygen of V_2O_5, further stabilizing the layered framework, while the carboxyl group weakens Zn^{2+}/V–O interactions, enhancing Zn^{2+} transport dynamics and lowering the energy barrier. Therefore, IO-V_2O_5 cathode achieves an impressive capacity (549.5 mAh g^{-1} at 0.2 A g^{-1}), fast ion diffusion coefficients (10^{-8}–10^{-7} cm^2 s^{-1}), excellent cycling stability (80.1% retention after 20 000 cycles at 30 A g^{-1}), and a remarkable energy density of 416.3 Wh kg^{-1}. This research by Liu group offers a promising pathway for developing high-capacity inorganic–organic co-intercalated V-based cathodes for next-generation AZIBs.

Conventional electrodes, concentration polarization induced by unbalanced charge transport and solid-state diffusion resistance significantly hinders reaction kinetics, limiting the practical application of AZIBs. To address this, Zhu *et al.*[99] proposed an integrated hybrid electronic–ionic conductor featuring spatially coupled charge transport pathways, enabling efficient redistribution and rapid of Zn^{2+} and electrons (Fig. 5e and f). Through vanadium oxide confinement, dual-conductive networks were self-assembled at the nanoscale, offering enhanced charge storage capability and accelerated ion diffusion within the bulk. This architecture not only increased the density of active sites and improved reaction kinetics but also mitigated proton-induced dissolution of the active material by enabling reversible ion transport during self-doping/dedoping processes. As a result, the tailored cathode (PEDOT-SO_3-ZnVO) demonstrated outstanding rate performance, delivering 310 and 148 mAh g^{-1} at 0.2 and 10 A g^{-1}, respectively, under a mass loading of 10 mg cm^{-2} (Fig. 5g and h). This work highlights a promising strategy for precisely tuning the electrochemical behavior of functional nanomaterials in high-performance AZIBs.

Constructing multiphase heterojunctions with tailored surface and interface properties offers a promising approach to address sluggish kinetics and limited redox activity. Yang *et al.*[100] developed a thermal oxidation strategy to fabricate a triphasic heterostructure composed of a VSSe core with VO_2 and V_2O_5-rich interfaces (Fig. 5i–k). The enlarged surface area and optimized interfacial coordination enhance electrode/electrolyte interactions and promote synergistic multi-anion (S/Se/O) and cation (V) redox reactions. Strengthened p–d orbital hybridization and spin polarization at the hetero-interface accelerate charge transfer and improve structural robustness. This integrated architecture overcomes the limitations of single-phase materials, enabling stable cycling and reliable operation even under harsh conditions. This study

presents a viable design strategy for versatile inorganic cathodes based on interfacial engineering of heterostructures.

3.2 Other V-based materials

Among the range of V-based cathode materials, $V_3O_7 \cdot H_2O$ has a mixed valence state (V^{5+}/V^{4+}), which has attracted considerable attention due to its layered structure and interlayer water. Compared with V_2O_5, it faces severe irreversible structural collapse and dissolution intercalation under repeated Zn^{2+} action, and further optimization is needed to achieve high-rate capability and long-term cycling durability. For example, Huang group proposed an effective strategy to address the rapid capacity fading of $V_3O_7 \cdot H_2O$ cathodes, which is typically caused by active material dissolution during cycling (Fig. 6a).[101] By doping high-valence Sn^{4+} into $V_3O_7 \cdot H_2O$ (referred to as Sn-$V_3O_7 \cdot H_2O$), they successfully enhanced the structural stability of AZIBs. The incorporation of Sn^{4+} thermodynamically reduced the formation energy of the host material and increased the dissolution energy of VO^{2+} ions, effectively mitigating vanadium loss (Fig. 6b and c). Moreover, Sn^{4+} doping improved electronic conductivity and broadened Zn^{2+} diffusion channels, thereby accelerating Zn^{2+} intercalation/deintercalation kinetics and boosting the overall electrochemical performance (Fig. 6d). In addition, composite with conductive materials is also an effective method to improve V_3O_7 cathode. Liu *et al.*[102] anchored a conductive metal–organic framework composed of Cu and hexahydroxy benzene ligands (Cu-HHTP) onto $V_3O_7 \cdot H_2O$ nanobelts *via* π–d conjugation. This anchored Cu-HHTP markedly enhanced the electrical conductivity of the $V_3O_7 \cdot H_2O$ nanobelts, enabling faster reaction kinetics and providing abundant active sites for efficient Zn^{2+} storage.

VO_2 is regarded as a prospective versatile inorganic cathode material for AZIBs owing to its unique tunnel or layered structures and the multivalent redox states of vanadium. However, unlike layered oxides with adjustable interlayer spacing, improving ion transport within tunnels of fixed dimensions remains challenging. Zhao and co-workers revealed that electrode architecture significantly influences tunnel orientation and thus ion diffusion kinetics (Fig. 6e).[32] Their study demonstrated that VO_2(B) nanoribbons with dispersed (001) facets preferentially align along the *c*-axis, enabling directional and rapid Zn^{2+} diffusion, which translates into superior rate performance and prolonged cycling durability. In contrast, aggregated VO_2(B) samples with random orientations exhibit isotropic and sluggish ion transport, resulting in poor electrochemical performance. These results highlight that regulating exposed crystal planes in combination with morphology-controlled electrode assembly provides a viable approach to optimize Zn^{2+} diffusion behavior in tunnel-type V-based cathodes.

Vanadate salts have attracted wide interest in AZIBs, as interlayer cations can expand spacing, suppress structural deformation, and enhance cycling stability. Their variable oxidation states further stabilize the framework and provide abundant Zn^{2+} storage sites, making sodium vanadate a highly promising anode candidate. Among various strategies, synthesis strategy mediated by guest materials has unique advantages. Hu *et al.*[103] developed $Na_2V_6O_{16} \cdot 1.63H_2O$ (H-NVO)

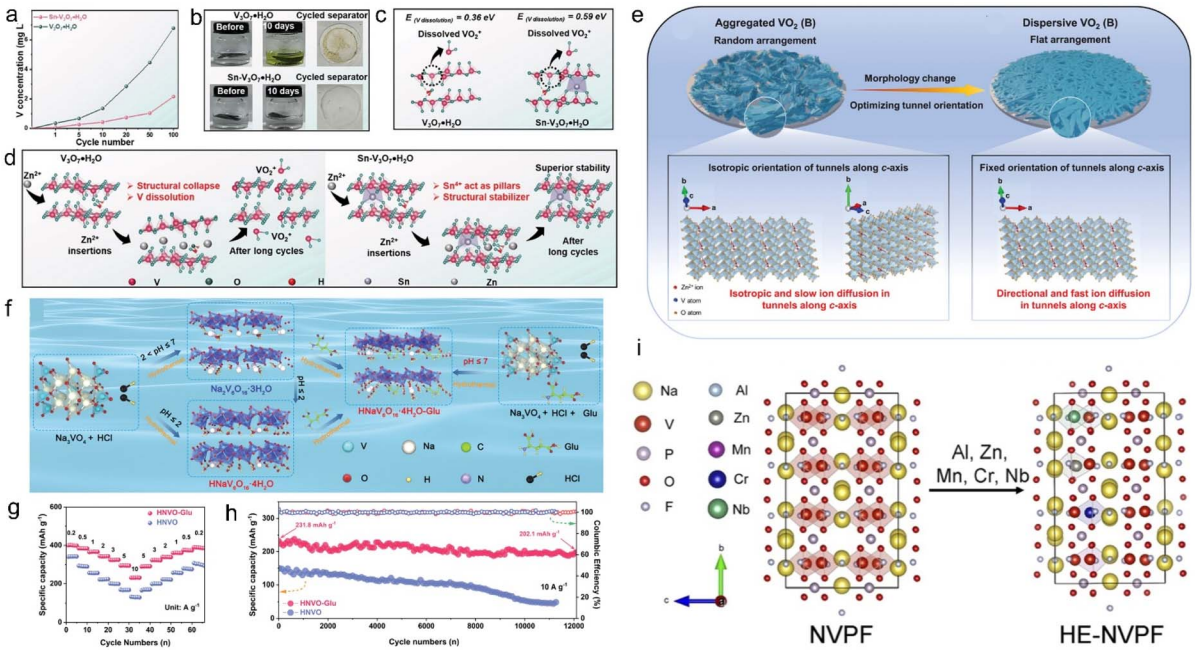

Fig. 6 V-based cathode modification strategies. (a) Solubility test, (b) post immersion image, (c) dissolution energy, and (d) cathodic stability schematic diagram of $V_3O_7 \cdot H_2O$ and Sn-$V_3O_7 \cdot H_2O$.[101] Copyright 2024, Wiley-VCH. (e) Schematic diagram of the influence of electrode arrangement related to material morphology on tunnel orientation and ion diffusion behavior.[32] Copyright 2024, Wiley-VCH. (f) Schematic illustration of the synthesis process. (g) Rate performance of HNVO-Glu. (h) Cycling stability.[104] Copyright 2024, Wiley-VCH. (i) NVPF@C and HE-NVPF@C crystal structure.[105] Copyright 2024, Elsevier.

nanowires exhibiting an electrical conductivity of 67 S m^{-1}. In the initial discharge phase, Zn^{2+} ions were incorporated into the host framework facilitated by water molecules, enabling reversible migration between the cathode and anode during subsequent cycles. The electrode demonstrated exceptional long-term stability, maintaining 90% of its initial capacity after 6000 cycles at a high current density of 5000 mA g^{-1}, with a retained capacity of 158 mAh g^{-1}. Although pre-inserted cations contribute to structural stabilization and enhanced ion transport kinetics, significant interlayer electrostatic interactions persist. To mitigate the strong electronegative environment imposed by oxygen atoms, the introduction of polar functional molecules can effectively modulate the local charge distribution. Zhang *et al.*[104] eveloped a guest-mediated strategy for synthesizing NVO, in which glutamic acid (Glu) was utilized to induce proton substitution of sodium, thereby achieving a crystalline transformation (Fig. 6f). This approach not only prevents structural phase transitions and collapse but also, *via* the polar groups on Glu, weakens the interaction between ions and the host material, thus enhancing the zinc-ion transport rate. The HNVO-Glu electrode therefore exhibited excellent cycle life of 12 000 cycles at a capacity retention of 87.2%.

The NASICON-type polyanionic compound with the general formula $M_3V_2(PO_4)_3$(M = Li, Na) possesses a stable 3D structure framework and represents a significant class of V-based materials for Zn^{2+} storage. Owing to their wide ion-conduction pathways and favorable ion transport kinetics, NASICON-structured compounds have emerged as promising versatile inorganic cathode candidates for AZIBs. Despite their potential, implementation is challenged by issues such as limited cycling stability, low intrinsic electronic conductivity, and sluggish Zn^{2+} diffusion. Among various modification strategies, cation doping has proven to be an effective approach to tailor the electrochemical properties and overcome these inherent limitations of NASICON-type cathodes. Liu group developed a high-entropy doped, carbon-coated NASICON-type $Na_3V_2(PO_4)_2F_3$ (HE-NVPF@C) cathode, through a rational high-entropy engineering strategy (Fig. 6i).[105] This work presents the first comprehensive experimental and theoretical investigation of charge storage mechanism in multi-component NASICON-type systems. The multi-element doping effectively suppresses Jahn–Teller distortion, minimizes structural deformation throughout Zn^{2+} (de)intercalation, and lowers the Zn^{2+} migration energy barrier, collectively enhancing cycling stability. Therefore, the cathode exhibits outstanding long-term durability, with an ultra-low-capacity decay rate of just 0.0031% after 6000 cycles at 20C. This high-entropy strategy offers a promising avenue for designing practical AZIBs with prolonged lifespan and high areal performance.

Overall, V-based compounds have become highly attractive multifunctional inorganic cathode materials in aqueous zinc ion batteries due to their diverse crystal structures, multi electron redox chemistry, and high theoretical specific capacity. However, its practical application is still limited by slow ion/electron transport, unstable structure (phase transition, interlayer collapse), and severe dissolution of vanadium in aqueous electrolytes. In recent years, Zn^{2+} has significantly improved the storage capacity, rate performance, and cycling stability of V-based cathodes through interlayer engineering (pre-insertion/co-insertion of metal cations and organic guests), construction of integrated electron/ion transport networks, and optimization of vanadium surfaces/interfaces. However, there are still several key challenges to be addressed in the future, including: how to effectively suppress the dissolution of VO_x without sacrificing the utilization rate of high valence vanadium; how to balance high load and structural integrity under actual high surface capacity conditions; and how to elucidate the coupling contributions of Zn^{2+}, H^+, pre-embedded cations, and structural water to the entire energy storage process.

Therefore, future research should focus on: (i) elucidating and actively regulating the synergistic storage pathways and water mediated structural evolution in multi ion (Zn^{2+}/H^+/M^+ (Li^+/Mg^{2+}/Al^{3+}, *etc.*)) layered/tunneling vanadate salts to achieve valence state transitions while avoiding side reactions; (ii) collaborative design of electrolyte interfaces for vanadium based cathodes, constructing specialized electrolyte systems and interface layers (such as buffering or weakly acidic media, coordination adjustable anions, functional additives, and artificial coatings), while suppressing vanadium dissolution and improving long-term cycling stability; (iii) expand the system beyond oxide systems, including vanadium nitride, sulfur/selenides, V–C complexes, and multi anionic multi-component frameworks, to construct a Zn^{2+}/H^+ synergistic energy storage framework with a wider voltage window and intrinsic stability; (iv) develop scalable and low-cost synthesis and densification processes to prepare vanadium based electrodes with high packing density and excellent mechanical stability, enabling them to operate stably under practical conditions such as high load, low electrolyte, and limited excess zinc, while considering safety, environmental friendliness, and recyclability. With the continuous development of these directions, V-based compounds are expected to play an important role in constructing high-energy density, long-life, and feasible AZIBs.

4 PBAs-based cathodes

Prussian blue analogues (PBAs) are promising versatile inorganic cathodes for AZIBs owing to their open framework (~10 Å), which enables wide Zn^{2+} diffusion channels and fast, reversible ion transport. Their robust structural integrity ensures long-term cycling stability, while a moderate operating voltage (0.9–1.2 V *vs.* Zn/Zn^{2+}) balances energy density and safety. Furthermore, the green, economically viable, and scalable aqueous synthesis of PBAs supports broad-scale application, highlighting their potential as next-generation high-performance versatile inorganic cathode materials.[106–108]

Due to the structural defects inherent in PBAs, their capacity deteriorates over long-term cycling. By doping with metal or non-metal ions, the crystal structure and electronic conductivity can be optimized, effectively improving cycling stability. Luo group developed Cu-substituted Mn-based Prussian Blue analogue (CuMn-PBA DSNBs) double-shelled nanoboxes *via* a surface modification and ion-exchange strategy, which

achieved excellent Zn^{2+} storage capability (Fig. 7a and b).[109] The distinctive hollow double-shell architecture provides abundant electroactive sites and effectively buffers the volume fluctuations during cycling. Furthermore, the partial doping of Cu and the resulting Mn vacancies are beneficial for reducing the Jahn–Teller distortion of the material octahedra, thereby contributing to improved cycling life (Fig. 7c). Yu group synthesized copper (Cu)-doped Mn PBA (CuMn PBA-2) hybrid architectures using water-based co precipitation technology. Adding Cu can partially improve the conductivity of the electrode and promote faster transport of Zn^{2+} within the electrode framework.[110]

The low utilization rate of active sites and abundant structural vacancies have always hindered the potential of PBAs. Zhang *et al.*[111] first used porous MXene as a multifunctional host material to improve the growth and crystallinity of PBAs (Fig. 7d). By targeted modification, CoHCF/MXene composite materials have achieved high surface area and low defects, resulting in impressive specific capacity cycle life. This synthesis strategy provides an effective method for inducing the growth of high surface area, low vacancy PBA-based materials for high-performance AZIBs. Pang team first reported an environmentally friendly and mild *in situ* generation and conversion strategy for synthesizing uniform V-based PBA nanocubes, using V_6O_{13} nanobelts as the vanadium source.[112] This method produced highly crystalline V-PBA nanocubes with ordered channels, enabling additional redox reactions associated with

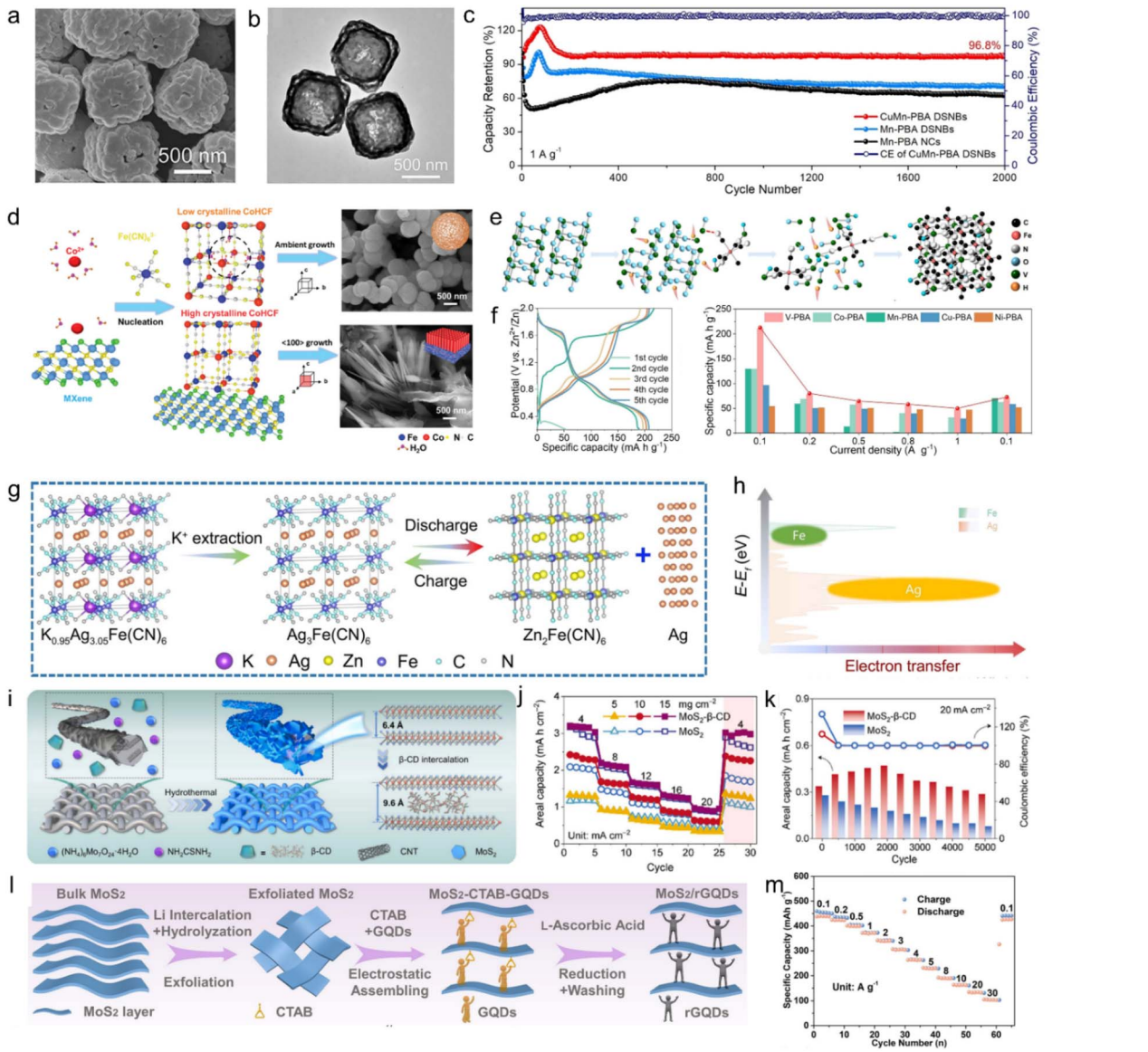

Fig. 7 Modification strategies for PBAs and TMD cathodes. (a) FESEM image, (b) TEM image, and (c) cycling performance of CuMn PBA DSNBs.[109] Copyright 2022, Wiley-VCH. (d) Nucleation and crystal growth processes.[111] Copyright 2024, Wiley-VCH. (e) Schematic diagram of the synthesis process of V-PBA. (f) Galvanostatic discharge curves and comparison of rate performance.[112] Copyright 2024, Wiley-VCH. (g) Schematic illustration of the energy storage mechanism and (h) redox potential of the AgHCF-3 electrode.[113] Copyright 2024, Wiley-VCH. (i) Schematic synthesis, (j) rate performance, and (k) cycling stability of MoS_2 and MoS_2-β-CD.[119] Copyright 2021, Elsevier. (l) Schematic synthesis and (m) rate capability of the MoS_2/rGQDs.[121] Copyright 2023, Wiley-VCH.

V^{3+}/V^{4+} and V^{4+}/V^{5+} couples (Fig. 7e). As a result, the as-prepared V-PBA achieved a superior specific capacity of approximately 200 mAh g^{-1}, outperforming conventional metal-based PBAs (M = Co, Cu, Mn, Ni) synthesized *via* co-precipitation (Fig. 7f).

To address the challenges of limited Ion transport kinetics and structural water in PBAs, Li group developed a defect-free and anhydrous silver hexacyanoferrate (AgHCF-3), by precisely tuning the K/Ag ratio within the framework (Fig. 7g).[113] Through two consecutive oxidation–reduction reactions (Fig. 7h), this material can accommodate nearly four electrons, delivering an electrochemical performance of 179.6 mAh g^{-1} at 20 mA g^{-1} while maintaining almost full coulombic efficiency. The reversible formation of Ag^0 during cycling contributes to excellent rate capability, maintaining 80.3% battery performance after long cycles. This study lays the foundation for designing PBAs cathodes that can provide high charge storage. Wang team prepared dislocation engineered potassium ferrocyanide (FeHCF) by using PVP additives, which reduced the crystal water content and induced crystal dislocations.[114] The low content of crystal water in FeHCF is related to the formation of dislocations. The dislocation effect effectively enhances the electrochemical reactivity and reaction kinetics of FeHCF. When used as a cathode, AZIBs exhibits a high voltage of 2.6 V, fast charging capability (<5 minutes), and satisfactory cycling stability.

In summary, PBAs is an attractive multifunctional inorganic cathode for AZIBs due to their open 3D framework, wide ion diffusion channels, and moderate voltage. Despite recent improvements in doping, defect strategies, and advanced host framework engineering, key challenges still exist, including how to simultaneously control vacancy concentration and crystal water to balance ion transport and structural stability, how to improve intrinsic conductivity without damaging the open framework, and how to suppress framework degradation and possible cyanide bridge dissolution under long-term cycling and high-quality loading. Therefore, future research should focus on: (i) atomic level regulation of defects, vacancies, and hydrochemistry to maximize the utilization of active sites while maintaining lattice integrity; (ii) reasonably design multi metal and multi electron PBA frameworks (such as adding high redox activity transition metals in addition to traditional Fe/Co/Mn) to overcome capacity limitations; (iii) electrolyte and interface synergistic engineering to stabilize PBAs electrolyte in real Zn^{2+}, reduce side reactions and structural decay; and (iv) developing scalable routes to achieve dense, mechanically robust, and even flexible PBAs electrodes that can operate under high area loads, poor electrolyte, and device related configurations. With continuous efforts in these directions, PBA is expected to develop from a model host material into a truly practical cathode for high-energy, fast charging, and durable.

5 Transition metal sulfide cathodes for AZIBs

Two-dimensional transition metal dichalcogenides (TMDs) have garnered significant attention as versatile inorganic cathodes materials due to their unique layered architectures, in which adjacent planes are maintained through weak interlayer van der Waals interactions.[115] This structural feature not only facilitates rapid charge carrier transport but also imparts mechanical flexibility, allowing the material to buffer the volumetric fluctuations associated with multivalent ion insertion and extraction. Additionally, their intrinsic semiconducting nature with tunable bandgaps supports efficient electron conduction. Among various TMDs, molybdenum disulfide (MoS_2) has emerged as a prototypical candidate for AZIBs, owing to its favorable electrochemical properties.[116–118] However, its inherent drawbacks including poor electrical conductivity, limited structural integrity, and rapid capacity fading continue to impede its practical deployment. Consequently, advanced strategies are required to lower Zn^{2+} intercalation energy barrier and enhance overall performance.

A novel approach was introduced by Liu and co-workers, employing oxygen mediated interlayer chemical coupling to significantly enhance the electrochemical behavior of MoS_2 cathodes in high load electrodes (Fig. 7i–k).[119] Inserting oxygen rich β-CD into the MoS_2 interlayer can promote the formation of oxygen mediated Mo–O and S–O bonds. This strategy not only effectively widens the interlayer spacing, but also reduces the coulombic interactions of Zn^{2+} with the layered structure, thereby endowing the anode with faster kinetics and stability. The poor diffusion kinetics of Zn^{2+} in MoS_2 remains a key challenge for its practical deployment. Jia *et al.*[120] developed a vertically stacked heterostructure of reduced graphene oxide (rGO) and mixed-phase MoS_2 (1T-2H) *via* a bottom-up assembly approach. The MoS_2/rGO vertical structure reduced the ion migration barrier and bandgap, thereby leading to enhanced Zn^{2+} migration and improved charge mobility. Consequently, the composite delivered a high capacity of 294.6 mAh g^{-1} at 0.2 A g^{-1} and excellent cycling stability with 96.8% retention after 1600 cycles at 3 A g^{-1}. This strategy offers a universal route for designing vertically stacked 2D heterostructures as high-performance AZIBs cathodes.

In order to improve the utilization of storage sites in MoS_2 and optimize storage performance, Liu group designed a MoS_2/reduced graphene quantum dot (rGQDs) hybrid with enlarged interlayer spacing, enhanced charge transport ability, wettability, and robust layered structure *via* electrostatic self-assembly (Fig. 7l).[121] The hybrid electrode, operated in a $ZnSO_4$ + 0.5 M $(NH_4)_2SO_4$ electrolyte, demonstrated a unique $Zn^{2+}/NH_4^+/H^+$ co-storage mechanism, where NH_4^+ and H^+ ions occupy interstitial sites between Zn^{2+} to fill inactive gaps and boost active site utilization. This synergistic "gap-filling" strategy significantly improved charge storage, enabling a superior electrochemical capacity of 439.5 mAh g^{-1} at 0.1 A g^{-1} and remarkable capacity retention of 89.7% after 8000 cycles (Fig. 7m). DFT calculations revealed that Zn^{2+} and NH_4^+ preferentially adsorb at octahedral and tetrahedral sites in the MoS_2 lattice, while H^+ prefers sulfur-top positions, supporting the multi-ion co-insertion behavior and validating the theoretical basis for enhanced electrochemical performance.

Featured with robust lamellar frameworks, WS_2 and VS_2 as composite partners are often integrated with metal sulfides to

give Zn^{2+}-accessible layered paths, improved electron conductivity and structural buffering for boosting Zn^{2+} storage. Xun *et al.*[122] grew enlarged-interlayer MoS_2 nanosheets on carbon cloth (CC) *via* further *in situ* WS_2 coating to form MoS_2@-WS_2@CC. Benefiting from the conductive CC networks and WS_2-expanded layers, it achieves enhanced ion diffusion and buffered volume changes to liberate high capacity (440 mAh g^{-1}) and life (200 cycles). Sun *et al.*[123] reported a self-constrained growth route to build rich-anion-vacancy VSSe/V_2CT_x heterostructures with multiscale V_2CT_x inner layer and selenized/sulfurized VSSe surface layer, which stabilize Zn^{2+} insertion/extraction, affording high capacity (350 mAh g^{-1}) and cycling life (10 000 cycles).

In conclusion, the optimization strategies for layered TMDs align closely with those employed for other two-dimensional materials, focusing on enhancing ion accessibility, electrical conductivity, and structural integrity. In future studies, advanced *in situ* and *operando* characterization techniques are expected to provide deeper insights into the relationship between interlayer structure evolution and electrochemical behavior, thereby clarifying Zn^{2+} storage mechanisms of TMD-based versatile inorganic cathodes. By integrating multiple modification approaches, such as doping, hybridization, interlayer engineering, and surface functionalization in a synergistic manner, it is anticipated that the performance limitations of layered TMDs can be effectively addressed, accelerating their practical application in high-performance AZIBs.

6 Halogen cathodes

Aqueous zinc–halide cathodes (Cl_2, Br_2, I_2) have attracted considerable attention, especially Zn–Br_2 and Zn–I_2 systems, due to their abundant resources, reversible anion-redox chemistry, wide operating voltages, and high theoretical capacities.[124,125] Unlike conventional cation-based batteries, these systems rely on halogen dissolution–deposition at the cathode and reversible Zn^{2+} plating at the anode. During oxidation, strong halogen–halogen interactions promote the formation of highly soluble polyhalides, which readily migrate and trigger severe shuttle effects, lowering coulombic efficiency and shortening cycle life. As a result, zinc–halide batteries mainly face two issues: (i) dissolution and shuttling of halide species and (ii) large polarization coupled with sluggish redox kinetics.

Halogen cathodes (Cl_2/Br_2/I_2/polyhalides) generally rely on the reversible redox conversion reactions during (dis)charge, which liberate high theoretical capacity, high operating voltage, and rapid redox kinetics, providing a powerful complementary for AZIBs.[125] However, halogen cathodes still face key challenges of shuttle, side reactions, and scale-up considerations. Specifically, soluble polyhalides (X_3^-/X_5^-) tend to migrate to the zinc anode under concentration gradient and electric field drive, leading to shuttle effects. The strong oxidizing properties of halogens can cause side reactions with electrolytes/electrodes, resulting in loss of active substances. In addition, the excellent performance of halogen cathodes is based on low mass loading (<2 mg cm^{-2}), which is far from the actual demand (>10 mg cm^{-2}). To address these issues, two efficient methods can be considered: (i) designing multi-level porous carbon/polymer hosts to fix halogens *via* physical confinement within micropores or cavities;[126,127] (ii) introducing chemical adsorption sites (*e.g.*, heteroatom doping, polar –OH/–COOH function groups, Zn/Fe metal coordination sites) into hosts to anchor polyhalides for reducing dissolution and improving reaction reversibility and stability.[128–130]

Therefore, designing halogen-confined host materials has become essential (Fig. 8). Focusing on structure and interface design is the core path to improve the performance of zinc halide batteries. Halogens have intrinsically low conductivity, resulting in poor redox reversibility and sluggish kinetics, and they are also unstable at room temperature, prone to volatilization and side reactions that cause active material loss and hinder practical use. Introducing halogen host materials with strong adsorption capacity is an effective way to address these issues. Through pore confinement and surface chemical adsorption, such hosts can spatially confine halogens/polyhalides and uniformly disperse them in the cathode. In this context, porous carbon materials with high conductivity and structural robustness are ideal halogen hosts, accommodating elemental halogens and polyhalide intermediates for high-performance zinc halide cathodes.

For example, Wu *et al.*[126] constructed a carbon-based framework PTCC900 using annealing strategy and assembled it as an iodine carrier to form the cathode of Zn–I_2 battery PTCC900@I_2 (Fig. 9a). This material constructs a multi-level pore network of nanopores (1.3–1.8 nm), which can achieve effective spatial confinement of I_2 and multi-iodine species. Additionally, the disordered graphite structure inside PTCC900 enhances electron transfer, significantly improving conductivity. Consequently, PTCC900@I_2 exhibits high capacity, excellent cycling stability, and outstanding rate performance.

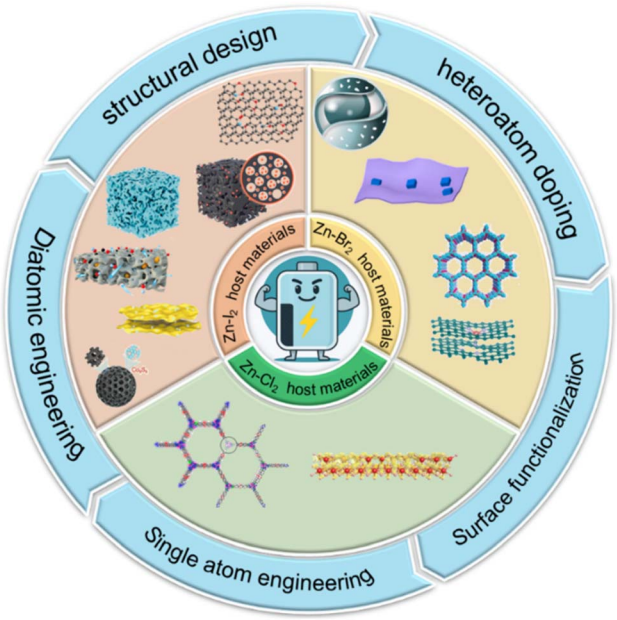

Fig. 8 Strategies for enhancing the performance of ZHBs through cathode regulation.

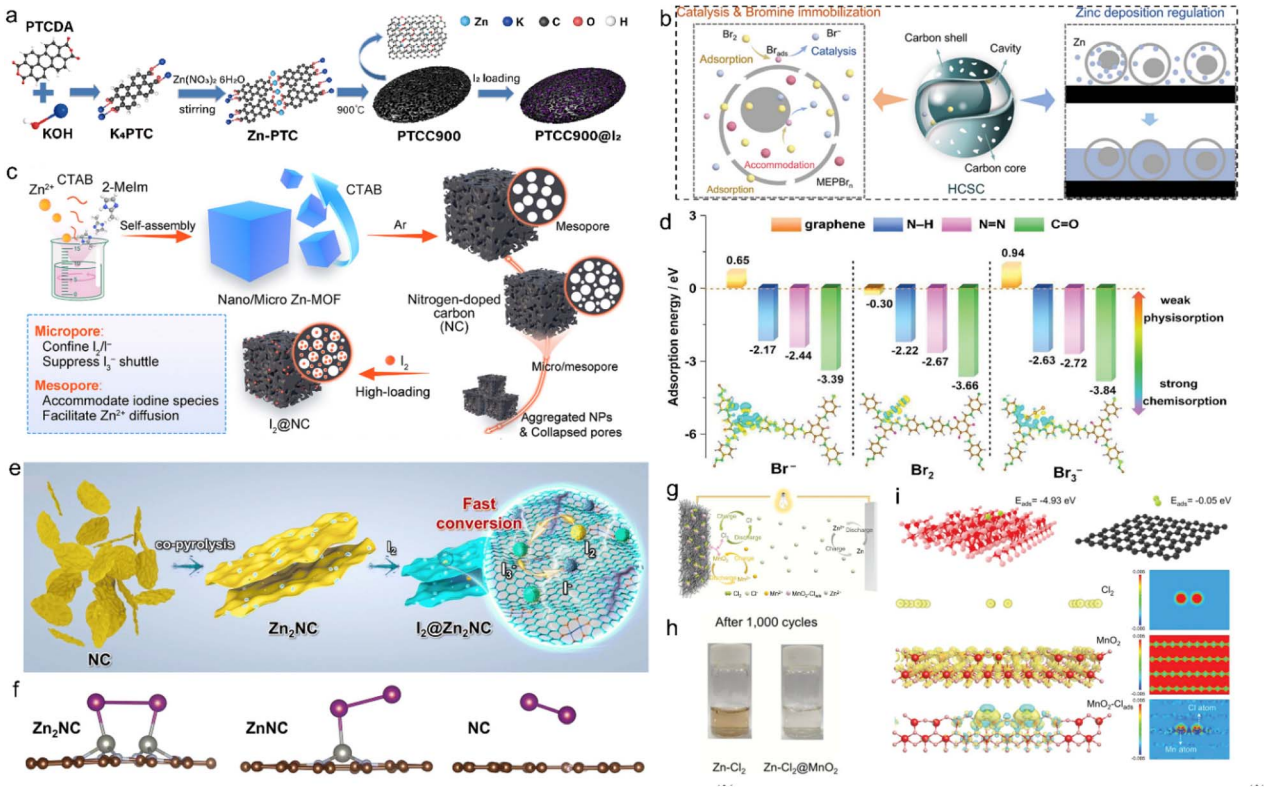

Fig. 9 Design strategies for halogen cathodes. (a) Schematic illustration of the synthesis of PTCC900@I_2.[126] Copyright 2023, Elsevier. (b) Schematic diagram of working mechanism.[131] Copyright 2025, Elsevier. (c) Schematic synthesis of cubic Zn-MOF derived NC and I_2@NC.[132] Copyright 2025, Wiley-VCH. (d) The adsorption energy and charge density patterns of different bromine compounds.[133] Copyright 2023, Elsevier. (e) Prepare the program and working mechanism diagram. (f) Density functional theory calculations.[135] Copyright 2025, Royal Society of Chemistry. (g) Schematic diagram of Zn–Cl_2@MnO_2 battery. (h) Photos of electrolyte after cycling. (i) Density functional theory calculations.[136] Copyright 2023, Wiley-VC.

However, it is still difficult to develop a carbon-based halogen matrix that provides both high conductivity and precise design while maintaining controllable halogen diffusion. Tang *et al.*[131] constructed hollow core–shell carbon nanospheres (HCSC) with an inner cavity structure based on the concept of structural confinement (Fig. 9b). This material has a developed hierarchical porous system, which can significantly enhance the specific surface area and bromine adsorption capacity of carbon felt, thereby endowing the electrode with higher catalytic activity. More importantly, by utilizing the adsorption and confinement effect of cavities on bromine, active bromine is effectively trapped inside the carbon spheres, significantly reducing the self-discharge behavior of the system. This work indicates that hollow carbon spheres as bromine-based materials provide a fresh structural control path for constructing excellent zinc halide batteries.

Relying solely on weak van der Waals interactions between pore walls and halides/polyhalides is insufficient to effectively suppress polyhalide shuttling. To strengthen polyhalide anchoring, heteroatoms such as oxygen, nitrogen, and sulfur, along with corresponding polar functional groups, are commonly introduced into the carbon framework to enhance halogen conversion efficiency and extend battery lifespan. Such heteroatom-regulated porous carbons, with increased polarity and tunable electronic structures, are regarded as highly promising halogen hosts because they significantly reinforce the interactions between the carbon matrix and halide ions. Pang group developed a nitrogen-doped carbon (NC) material derived from Zn-MOF as a cathode host for aqueous Zn–I_2 batteries.[132] CTAB, acting as a surfactant and capping agent, regulates the growth of Zn-MOF nanocubes. The resulting high surface area micropores enhanced the conversion kinetics of iodine, suppressed the I_3^- shuttle effect, and provided abundant active sites (Fig. 9c). Mesopores further improve iodine accommodation and facilitate electron/ion transfer. Additionally, pyridine-*N*/graphite-*N* doping aids iodine species adsorption and conversion. I_2@S3-1000 cathodes exhibit excellent long-term cycling stability due to these benefits.

Sun *et al.*[127] proposed a dual-doping strategy with boron and nitrogen to locally regulate the electronic environment of carbon hosts, thereby boosting Zn–I_2 battery performance. Combined experimental and DFT results indicate that N–B sites effectively suppress the shuttle effect, strengthen interactions with iodide species, and accelerate their catalytic conversion kinetics. Wang *et al.*[128] fabricated a Prussian blue-modified nitrogen-doped carbon (PB@NC) composite *via* a simple anion-exchange route and loaded it onto a carbon membrane. The nitrogen-doped carbon provides high conductivity and

strong adsorption toward bromine species, enabling efficient electron transport and local bromine enrichment at the reaction interface. Under the electronic assistance of NC, Prussian blue can rapidly switch between oxidized and reduced states, then selectively engage in redox reactions with Br_2. This offers an alternative bromine redox pathway, markedly accelerating electrochemical kinetics and realizing targeted, reversible redox catalysis.

The non-polar carbon skeleton only provides weak physical adsorption, which is not sufficient to effectively suppress the shuttle of polyhalides. In contrast, host materials with polar functional groups can form stronger interactions with halide ions through chemical adsorption or hydrogen bonding, thereby anchoring polyhalides on the cathode surface, limiting their dissolution and diffusion in the electrolyte, and ultimately extending battery life. For example, Zeng *et al.*[129] developed asphalt-derived carbon (PPC_{MK}) with a microporous structure and abundant oxygen groups (C=O, –COOH, –OH) using a one-step method to create iodine-based cathodes (I_2/PPC_{MK}). The micropores in PPC_{MK} efficiently prevent I_2 dissolution and I_3^- formation, while its high surface area boosts iodine loading. DFT calculations show that the oxygen groups (C=O, –COOH, –OH) in PPC_{MK} strengthen the adsorption of free I_3^- through strong chemical interactions. Due to its dual iodine-confining mechanism, PPC_{MK} maintains excellent stability under both standard and high-load conditions. Indeed, COFs are more closely related to organic material systems and thus cannot be classified as an inorganic material. It should be pointed out that COFs are often selected as the redox-nonactive supporter materials for loading halogen cathodes (*e.g.*, I_2/Br_2, polyhalides), which can effectively anchor halogen species to suppress their dissolution/shuttling and provide fast interfacial ion/electron transport paths. Liu and co-worker constructed a trifluoromethyl-functionalized covalent organic framework (F-COF) as an iodine host to suppress the shuttle effect.[133] The strong electron-withdrawing trifluoromethyl functional groups redistribute charge in the COF backbone, enhancing iodine uptake and stabilizing polyiodide species. Theoretical calculations confirm that F-COF exhibits strong adsorption toward polyiodides, effectively inhibiting their migration (Fig. 9d). Consequently, Zn–I_2 batteries employing F-COF as the iodine host deliver highly reversible behavior and ultralong cycling stability (40 000 cycles at 50C).

Building efficient catalysts is an important way to achieve high energy density and long lifespan of zinc–halide cathodes. Metal catalysts accelerate halogen oxidation-reduction by adjusting X–X (X = I, Br, Cl) bond structure and reducing the conversion energy barrier, and are therefore commonly introduced as carbon-based hosts to enhance electrochemical performance. For example, Zhi group designed a mesoporous carbon-based conductive bromine host (FeSAC-CMK) in which isolated iron single atoms (FeN_5 sites) are coordinated by nitrogen.[130] These FeN_5 centers can strongly immobilize neutral bromine (Br^0), effectively suppress the formation of Br_3^-, and bifunctionally catalyze the Br^-/Br^0 redox conversion. By releasing one-third of Br^- that would otherwise be locked in Br_3^- complexes, FeN_5 sites enhance bromine utilization and reversibility. As a result, Zn–Br_2 batteries equipped with this dual-functional catalytic host achieve higher discharge capacity, elevated voltage plateau, improved rate performance, and prolonged cycling life. Tulchinsky *et al.*[134] constructed and verified a cobalt MOF based on N-containing imidazole ligands, in which unsaturated Co(II) sites are quantitatively oxidized by halogens to form stable solids bearing terminal Co(III)–halogen bonds. Upon thermal treatment, these Co(III)–halogen bonds undergo homolytic cleavage, regenerating Co(II) and releasing elemental halogen. This work clarifies how MOFs can confine and reversibly adsorb halogen species, and provides a viable route to designing $ZnCl_2$ cathodes with high safety, reversibility, and performance.

Although single metal atom catalysts exhibit excellent activity in the zinc–halide cathodes system, they often face stability issues such as atomic aggregation and active site leaching under actual working conditions. On the other hand, they are also inherently limited by scaling relationships: enhancing the adsorption of one reactant often weakens the binding ability to another intermediate. This contradiction is particularly prominent in Zn–I_2 batteries, where multiple intermediate species such as I^-, I_3^-, I_5^-, and I_2^- have significantly different affinities for catalytic sites, making it difficult for a single metal center to simultaneously achieve optimal regulation of each reaction step. Based on this, bimetallic catalysts exhibit greater design freedom and outstanding comprehensive catalytic performance in multi-step halogen conversion reactions due to their adjustable bimetallic synergistic effect and richer charge interaction modes. Mai and co-workers developed honeycomb-like Zn–Zn dual-metal sites anchored on N-doped carbon nanosheets *via* a novel co-pyrolysis strategy to serve as iodine host centers, as confirmed by microscopic and spectroscopic characterization (Fig. 9e).[135] Electrochemical tests combined with theoretical calculations reveal that these Zn_2 sites not only strengthen I_2 adsorption but also accelerate multi-iodide redox kinetics (Fig. 9f). Consequently, the I_2@Zn_2NC cathode delivers high capacity and ultralong cycling durability, sustaining 100 000 cycles at 50C.

In order to further improve the interfacial charge transfer ability and catalytic performance of host materials, metal compounds have been introduced to create structures for rapid electron transfer. Chen group abandoned traditional carbon hosts and instead employed a low-cost MnO_2 redox adsorbent to regulate Cl_2 electrochemistry (Fig. 9g and h).[136] DFT calculations and kinetic analysis reveal that the intermediate Cl_{ads}@MnO_2 acts as an electron donor, accelerating electrode kinetics and Cl_2 reduction while contributing to capacity enhancement (Fig. 9i). Benefiting from the synergistic interaction of Mn^{2+}/MnO_2 with chlorine during both dis(charge), the Zn–Cl_2@MnO_2 battery shows improved reaction dynamics, coulombic efficiency, and cycling stability. This Cl_2 cathode regulation strategy provides a methodological approach for the research of aqueous Zn–Cl_2 batteries.

To further expand the application scope of limited catalytic strategies in halogen hosts, Liang group developed a Co_9S_8@-nitrogen-doped carbon catalyst with an anti-perovskite structure.[137] This design allows Co_9S_8 nanoparticles to be uniformly

confined within a porous honeycomb-like N-doped carbon framework. Besides, the Co_9S_8 phase features an electron-deficient character, which induces strong electrostatic attraction and robust anchoring toward iodine species. As a result, the Co_9S_8@NC catalyst delivers a high energy density of 554 Wh kg^{-1} and maintains stable cycling performance over 5000 cycles.

Although the current design strategy for halogen materials has made progress, it still faces several challenges: (i) insufficient regulation of the pore structure in carbon materials makes it difficult to simultaneously achieve sufficient electrolyte infiltration, charge transfer, and full exposure of storage sites; (ii) although surface functionalization can improve halogen anchoring, precise control of functional group sites remain difficult, which may result in uneven electrode surface reactions; (iii) many carbon-based materials are difficult to achieve precise control over the electronic structure and conversion pathways of halogen species due to physical limitations. In the future, electron rich regions should be introduced by doping heteroatoms, optimizing interface polarity, ion distribution, and creating ordered hierarchical pore structures to effectively improve ion transport efficiency. Meanwhile, metal atom doping can enhance the adsorption and catalytic performance of halogen substances, suppress shuttle effects, and accelerate redox reactions. The doping of heteroatoms still faces problems such as unclear regulatory mechanisms and decreased conductivity. In the future, *in situ* characterization and theoretical calculations should be strengthened, and multi-component co-doping schemes should be explored to enhance the confinement, catalytic, and conductive capabilities of iodine species, and promote the development of Zn–halogen batteries.

7 Summary and outlook

This article reviews the latest developments in versatile inorganic cathodes for AZIBs, covering major categories such as Mn-based materials, V-based materials, PBAs, transition metal sulfides, and emerging halogen cathodes. There are three charge-storage mechanisms in inorganic cathodes for AZIBs: Zn^{2+} storage, H^+ storage, and H^+/Zn^{2+} co-storage, resulting in different electrochemical performances. Zn^{2+} ion (or hydrated structures) is a typical charge carrier, but its large hydrated size and high desolvation energy trigger slow interfacial reaction. In contrast, the smallest-radius H^+ can transfer along the H-bonding network of water, and enter the interlayer of inorganic cathodes to achieve fast charge storage, but is prone to corrode inorganics, resulting in inferior cycling stability of AZIBs. Significantly, H^+/Zn^{2+} co-storage enables fast charge compensation to mitigate polarization, and contributes to superior reversible (de)insertion energy storage, thereby synergistically enhancing the capacity and rate performance of AZIBs.

The key performance indicators of these materials in battery systems, such as discharge capacity, rate capability, energy density, and cycling stability, are compared. Table 1 summarizes the key performance characteristics of versatile inorganic cathode materials based on the semi-quantitative rationale. The electrochemical performances of various inorganic cathode materials were compared by prioritizing literature results tested under identical conditions for AZIBs (electrolyte: $ZnSO_4/H_2O$ and $Zn(OTF)_2/H_2O$ solution; voltage window: 0∼1.8 V; mass load: 1∼2 mg cm^{-2}; current density: 0.1∼0.5 A g^{-1}). Mn-based cathodes often exhibit large interlayer spacing to achieve high Zn^{2+} diffusion coefficient ($D_{Zn^{2+}}$, 10^{-15}∼10^{-4} cm^2 s^{-1}). In contrast, the interaction between Zn^{2+} and V–O in V-based cathodes are stronger, resulting in a decrease in $D_{Zn^{2+}}$ (10^{-11}∼10^{-6} cm^2 s^{-1}). Although PBAs have open 3D channels, the transport of Zn^{2+} is limited by the influence of structural water, resulting in relatively low $D_{Zn^{2+}}$ (10^{-15}∼10^{-9} cm^2 s^{-1}). Compared with layered Mn/V-based cathodes, layered TMDs often show low $D_{Zn^{2+}}$ (10^{-10}∼10^{-8} cm^2 s^{-1}) due to narrower ion channels.

Table 1 compares various inorganic cathode materials and emphasizes their inherent trade-off between capacity and cycling durability in AZIBs. Specifically, compared with pristine MnO_2, multivalent redox chemistry endows Mn-based oxides with high capacity (230–400 mAh g^{-1}). However, the Jahn–Teller distortion results in structural pulverization of Mn-based cathodes, accelerating performance degradation during long-term cycling. In contrast, the modified V-based oxides with more open and stable layered V–O frameworks deliver better capacity (310–500 mAh g^{-1}) compared to V_2O_5. In addition, modified PBAs with open 3D channels generally exhibit good cycling stability (∼10 000 cycles) compared with pristine CuHCF, but face slow ion transport and low capacity (80–200 mAh g^{-1}). Featured with good structural elasticity, compared with pristine MoS_2, TMDs exhibit high capacity (200–400 mAh g^{-1}). However, during the long cycle process, TMDs often undergo structural degradation, leading to increased polarization and subsequently a decrease in cycle life (1000–8000 cycles). Different from the abovementioned insertion-type metal compounds, conversion-type halogens activate multielectron redox pairs to deliver good capacity (200–400 mA h g^{-1}) and long cycle life.

Overall, progress has been made in the development of inorganic cathodes, with each type of material possessing unique structural advantages and electrochemical properties. But several key challenges must be addressed to accelerate the development of versatile inorganic cathode materials for next-generation AZIBs.

(i) In practical conditions, Mn/V oxides, PBAs, TMDs and halogen materials in AZIBs typically use the mass loading of 1∼2 mg cm^{-2} in cathodes, excess Zn metal anodes (diameter: 14 mm; thickness: 50∼100 μm), electrolyte amount (∼120 μL), cutoff voltage window (V oxides/TMDs: 0.2–1.6 V; Mn oxides/PBAs/halogen: 0.8–1.9 V), and long-term stability metrics (3000∼10 000 cycles). Under these consolidated condition, different inorganic materials show differential electrochemical performances benefiting from their respective structural features, which provide feasible and useful platforms to propel the future development of next-generation energy communities.

(ii) Cathodic optimization. In addition to existing modification methods, it is particularly urgent to develop innovative strategies to enhance the performance of versatile inorganic cathodes. Meanwhile, the diffusion of Zn^{2+} in the cathode is

Table 1 Comparison of electrochemical properties of AZIBs with different cathodes

Materials	Mass loading (mg cm^{-2})	Electrolyte	Voltage (V)	Capacity (mAh g^{-1})	Current (A g^{-1})	Cycles	Retention rate (%)	Current (A g^{-1})	Ref.
Mn-based compounds									
α-MnO_2	N/A	1 M $ZnSO_4$	1–1.8	197	0.13	75	50	0.084	62
NS-MnO_2	1.5	2 M ZnSO4 + 0.1 M $MnSO_4$	0.8–1.8	284	0.2	1500	94	1	69
$Ce_{in/inter}$-MnO_2	1–2	2 M $ZnSO_4$ + 0.1 M $MnSO_4$	0.9–1.8	270.9	0.3	2000	100	3	70
$Al_{0.1}$–MnO_2	1.5	2 M $ZnSO_4$ + 0.1 M $MnSO_4$	0.8–1.8	347.6	0.1	1000	87	1	71
HE-MnO/C	1–1.5	2 M $ZnSO_4$ + 0.2 M $MnSO_4$	0.2–1.8	230.2	0.3	10 000	92.3	10	72
KMO-NAPD	2	2 M $ZnSO_4$ + 0.4 M $MnSO_4$	0.8–1.9	233	1	1000	85	4	73
DP-MnO_2	1.5	2 M $ZnSO_4$ + 0.1 M $MnSO_4$	1–1.8	357	0.1	1000	N/A	1	74
3DP MnO_2	2.7	1 M $ZnSO_4$ + 0.1 M $MnSO_4$	1–1.8	288.8	N/A	N/A	N/A	N/A	75
C-MnO_2	1.5	2 M $ZnSO_4$ + 0.2 M $MnSO_4$	0.6–1.8	302	0.2	10 000	78	5	76
γ-MnO_2@CP	2	2 M $ZnSO_4$ + 0.1 M $MnSO_4$	0.8–1.8	391.2	0.1	3000	92.1	5	77
VMn-Mn_3O_4@C	1.5	2 M $ZnSO_4$ + 0.2 M $MnSO_4$	1–1.8	280.9	0.1	5000	100	1	83
$Zn_{0.17}MnO_{2-n}\cdot 0.52H_2O$	1.5	2 M $ZnSO_4$ + 0.2 M $MnSO_4$	0.8–1.9	558	0.1	5000	95.8	5	84
NC@VN/MnO	1.5	2 M $ZnSO_4$ + 0.2 M $MnSO_4$	0.7–1.8	550	0.2	12 000	83	10	85
$Zn_{0.5}Mn_2O_4$	1	3 M $ZnSO_4$ + 0.2 M $MnSO_4$	1–1.8	299	0.1	3200	92	10	86
V-based compounds									
V_2O_5	N/A	3 M $ZnSO_4$	0.4–1.4	224	0.1	400	54	2	91
$M_xV_2O_5\cdot nH_2O$	1.5	2 M $Zn(OTF)_2$	0.2–1.6	N/A	N/A	1000	88.4	0.2	89
IO-V_2O_5	1.5	3 M $Zn(OTF)_2$	0.2–1.6	549.5	0.2	20 000	80.1	30	98
PEDOT-SO_3-ZnVO	1.5	2 M $ZnSO_4$	0.2–1.6	310	0.2	5000	90.3	5	99
VSSe/VO_2/V_2O_5	1–1.2	3 M $Zn(OTF)_2$	0.1–1.7	432	1	12 000	60	10	100
Sn-$V_3O_7\cdot H_2O$	1.5	3 M $Zn(OTF)_2$	0.4–1.5	408	0.1	6000	89.3	5	101
Cu-HHTP	2	3 M $Zn(OTF)_2$	0.2–1.6	518	0.2	5000	81	10	102
VO_2(B)	1	3 M $Zn(OTF)_2$	0.2–1.5	420.8	0.1	5000	84.3	10	32
H-NVO	1.5	3 M $Zn(OTF)_2$	0.2–1.6	352	0.05	6000	90	5	103
HNVO-Glu	1.5	3 M $Zn(OTF)_2$	0.2–1.6	354.6	1	12 000	87.2	10	104
HE-NVPF@C	10	1.7 M $Zn(OTF)_2$	0.8–1.9	74.1	0.5	6000	81	20	105
Prussian blue analogues									
CuHCF	N/A	2 M $ZnSO_4$	0.45–1.4	53	0.06	100	96.3	N/A	108
CuMn-PBA DSNBs	1	2 M $Zn(OTF)_2$	0.5–1.8	116.8	0.1	2000	96.8	1	
CuMn PBA-2	1.2	2 M $ZnSO_4$ + 0.2 M $MnSO_4$	0.7–1.9	175	0.5	2000	N/A	3	
CoHCF/M-1%	1.2–1.5	15 M $ZnCl_2$	0.7–2.0	197	0.1	3000	95.3	2	
V-PBA	1	3 M $Zn(OTF)_2$	0.2–2.0	120.7	0.5	10 000	55	10	
AgHCF-3	2	1 M $ZnSO_4$	0.5–2.0	79.6	0.02	100	90.3	0.2	
Transition metal sulfides									
MoS_2	N/A	3 M $Zn(OTF)_2$	0.2–1.4	21	0.1	N/A	N/A	N/A	118
MoS_2-β-CD	10	2 M $ZnSO_4$	0–1.4	228	4	5000	85.3	20	119
MoS_2/rGO	1.5–2.0	3 M $Zn(OTF)_2$	0.2–1.5	294.6	0.2	1600	96.8	3	120
MoS_2/rGQDs	2–3	1 M $ZnSO_4$ + 0.5 M $(NH_4)_2SO_4$	0.2–1.5	439.5	0.1	8000	89.7	10	121
VSSe/V_2CT_x	3	3 M $Zn(OTF)_2$	0.3–1.6	355	0.2	10 000	51	10	123

Table 1 (*Contd.*)

Materials	Mass loading (mg cm^{-2})	Electrolyte	Voltage (V)	Capacity (mAh g^{-1})	Current (A g^{-1})	Cycles	Retention rate (%)	Current (A g^{-1})	Ref.
Halogens									
PTCC900@I_2	N/A	2 M $ZnSO_4$	0.8–1.6	242	0.1	50 000	45	5	126
I_2@S3-1000	N/A	2 M $ZnSO_4$	0.6–1.6	208.5	0.05	10 000	81	2	132
I_2/PPC_{MK}	1.5–2.5	2 M $ZnSO_4$	0.5–1.6	236	0.21	20 000	85	4.4	129
F-COF	N/A	3 M $ZnSO_4$	0.8–1.9	275	0.5	1000	83	2	133
FeSAC-CMK	1	2 M $ZnSO_4$ + 0.1M Br_2	1–1.9	344	0.2	2000	76	2	134
I_2@Zn_2NC	N/A	2 M $ZnSO_4$	0.6–1.8	212	0.5C	100 000	N/A	50C	135
I/Co_9S_8@NC	N/A	7.5 m $ZnCl_2$	0.6–1.8	458	1	5000	N/A	5	137

often limited by strong electrostatic interactions. Therefore, in the future, it may be considered to introduce low electronegativity materials or form a three-dimensional framework structure to alleviate the dynamic bottleneck caused by strong electrostatic interactions. In addition, exploring new stable cathode material systems, such as bismuth based or metal phosphide materials, will provide feasible high-performance solutions for large-scale AZIBs.

(iii) Electrolyte engineering design. Traditional aqueous electrolytes are limited by a narrow electrochemical stability window, making it difficult to support higher operating voltages and energy outputs. Therefore, it is necessary to expand the "available window" by regulating the solvation structure and ionic environment. For example, ultra-high concentration electrolytes, deep eutectic systems, and water/organic mixed electrolytes are expected to achieve higher potential operation while suppressing side reactions and active substance dissolution; at the same time, introducing functional additives can optimize the behavior of the electrode/electrolyte interface, weaken adverse processes such as hydrogen evolution and organic component decomposition. Further, the development of gel polymer and all solid electrolyte is expected to significantly improve flexibility and safety on the premise of ensuring ion conduction, providing new design space for zinc ion batteries for wearable energy storage devices.

(iv) Although significant efforts have been made to explore future applications of high-mass-loading inorganic cathodes, their scalable, reproducible, and cost-effective fabrication with desirable electrochemical properties are still challenging. Most reported excellent properties of inorganic cathodes are based on the low mass loading (<2 mg cm^{-2}), which is far away from the practical level (>10 mg cm^{-2}). It is thus of great importance to explore new techniques to extend the production scale of sustainable inorganic cathodes from the laboratory stage to the practical industrial level.

(v) The future routes of developing high-energy-density AZIBs should be focused on the collaborative enhancement of capacity and voltage in high-mass-loading inorganic cathodes: (i) increasing the redox-site density (*e.g.*, constructing rich lattice defects, expanding interlayers) and improving electron/ion transport (*e.g.*, introducing conductive substrates, rich porosity within inorganics) for achieving desirable capacity storage; (ii) elevating redox potentials within stable electrochemical windows (*e.g.*, introducing polyanions within inorganic lattices, heteroatom substitution).

(vi) AI intelligence and representation. In multi-coupled inorganic electrode systems, structural evolution and reaction pathways are often highly complex, making it difficult to fully elucidate their working mechanisms within a single disciplinary framework. This calls for closer integration of materials chemistry, electrochemistry, theoretical modeling, and data science, with tight coupling between experiments and simulations. At the same time, *in situ* and quasi *in situ* characterization techniques, such as synchrotron X-ray methods, *in situ* Raman and infrared spectroscopy, and time-resolved electrochemical impedance analysis are essential for tracking phase transitions, interfacial reconstruction, and ion migration pathways under

realistic operating conditions, thereby providing mechanistic guidance for the rational design of high-performance electrodes. Furthermore, the combination of machine learning, automated high-throughput experimentation, and intelligent optimization algorithms is expected to rapidly identify promising electrode/electrolyte pairs within a vast compositional and structural space, significantly shortening the cycle from conceptual design to device validation and accelerating the iterative development of next-generation zinc-based energy storage systems.

(vii) Sustainable development and feasibility. The synthesis of high-performance multifunctional inorganic cathode materials often relies on complex processes such as multi-step precursor design, strict atmosphere control, or high-temperature long-term annealing, which not only increases energy consumption and equipment requirements, but also weakens the repeatability of the process and the feasibility of large-scale production. Therefore, developing green, low-cost, and process scalable synthetic routes (such as aqueous/solvothermal synthesis, low-temperature solid-phase reactions, and resource reuse based on biomass or industrial by-products) is crucial for achieving a balance between electrochemical performance, preparation costs, and environmental sustainability. In the future, we should also pay attention to process compatibility and engineering feasibility, such as matching with existing battery manufacturing processes such as coating, rolling, 3D printing, and electrode roll to roll production. This is expected to promote the development of multifunctional inorganic cathodes from laboratory concepts to large-scale, low-cost practical applications.

Author contributions

Conceptualization, Kang Guo, Yaokang Lv, Ziyang Song, Lihua Gan, Mingxian Liu; writing – original draft preparation, Kang Guo; figure and table preparation, Kang Guo; writing – review and editing, Ziyang Song, Lihua Gan, Mingxian Liu. All authors have read and agreed to publish the version of manuscript.

Conflicts of interest

The authors declare no conflicts of interest.

Data availability

The data that support the findings of this study are available on request from the corresponding author, upon reasonable request.

Acknowledgements

This work is financially supported by the National Natural Science Foundation of China (No. 22272118, 22172111, and 22309134), the Shanghai Rising-Star Program (23YF1449200), the Zhejiang Provincial Science and Technology Project (2022C01182), and the Fundamental Research Funds for the Central Universities.

Notes and references

1 B. Dunn, H. Kamath and J. M. Tarascon, *Science*, 2011, **334**, 982.
2 M. Armand and J.-M. J. N. Tarascon, *Nature*, 2008, **451**, 652–657.
3 S. Zhao, Y. Zhang, J. Li, L. Qi, Y. Tang, J. Zhu, J. Zhi and F. Huang, *Adv. Mater.*, 2023, **35**, 202300195.
4 P. D. Lund, *Joule*, 2020, **4**, 2543–2545.
5 J. Deng, C. Bae, A. Denlinger and T. Miller, *Joule*, 2020, **4**, 511–515.
6 A. Huang, J. Xu, Y. Huang, G. Chu, M. Wang, L. Wang, Y. Sun, Z. Jiang and X. Zhu, *Acta Phys. Chim. Sin.*, 2025, **41**, 100037.
7 M. R. Palacín, *Chem. Soc. Rev.*, 2018, **47**, 4924–4933.
8 J. Liu, Z. Zhang, M. Kamenskii, F. Volkov, S. Eliseeva and J. Ma, *Acta Phys. Chim. Sin.*, 2025, **41**, 100011.
9 C. M. Costa, J. C. Barbosa, R. Gonçalves, H. Castro, F. J. D. Campo and S. Lanceros-Méndez, *Energy Storage Mater.*, 2021, **37**, 433–465.
10 M. S. Whittingham, *Nano Lett.*, 2020, **20**, 8435–8437.
11 H. Bajolle, M. Lagadic and N. Louvet, *Energy Res. Social Sci.*, 2022, **93**, 102850.
12 L. F. Zhao, Z. Hu, W. H. Lai, Y. Tao, J. Peng, Z. C. Miao, Y. X. Wang, S. L. Chou, H. K. Liu and S. X. Dou, *Adv. Energy Mater.*, 2020, **11**, 202002704.
13 P. K. Nayak, L. Yang, W. Brehm and P. Adelhelm, *Angew. Chem., Int. Ed.*, 2017, **57**, 102–120.
14 Y. Gao, Q. Yu, H. Yang, J. Zhang and W. Wang, *Adv. Mater.*, 2024, **36**, 2405989.
15 H. Zhang, Y. Gao, X. Liu, L. Zhou, J. Li, Y. Xiao, J. Peng, J. Wang and S. L. Chou, *Adv. Energy Mater.*, 2023, **13**, 2300149.
16 Y. Zheng, Y. Meng, X. Hu, H. Peng, L. Feng, Y. Wang and B. Li, *Adv. Mater.*, 2024, **37**, 2413202.
17 Y. Wang, Z. Cao, Z. Du, X. Cao and S. Liang, *Acta Phys. Chim. Sin.*, 2025, **41**, 100035.
18 H. Zhang, X. Liu, H. Li, I. Hasa and S. Passerini, *Angew. Chem., Int. Ed.*, 2020, **60**, 598–616.
19 Y. Liang and Y. Yao, *Nat. Rev. Mater.*, 2022, **8**, 109–122.
20 D. Chao, W. Zhou, F. Xie, C. Ye, H. Li, M. Jaroniec and S.-Z. Qiao, *Sci. Adv.*, 2020, **6**, eaba4098.
21 M. Huang, X. Wang, J. Wang, J. Meng, X. Liu, Q. He, L. Geng, Q. An, J. Yang and L. Mai, *Angew. Chem., Int. Ed.*, 2023, **62**, e202308961.
22 D. Xie, Y. Wang, L. Tian, H. Huang, J. Sun, D. W. Kim, J. Zhao and J. Mao, *Adv. Funct. Mater.*, 2024, **35**, 2413993.
23 J. Wei, P. Zhang, J. Sun, Y. Liu, F. Li, H. Xu, R. Ye, Z. Tie, L. Sun and Z. Jin, *Chem. Soc. Rev.*, 2024, **53**, 10335–10369.
24 K. Du, Y. Liu, Y. Zhao, H. Li, H. Liu, C. Sun, M. Han, T. Ma and Y. Hu, *Adv. Mater.*, 2024, **36**, 2404172.
25 X. Zhang, R. Wang, Z. Liu, Q. Ma, H. Li, Y. Liu, J. Hao, S. Zhang, J. Mao and C. Zhang, *Adv. Energy Mater.*, 2024, **14**, 2400314.
26 Y. Fu, Y. Zhang, Q. Huang, P. Liu, Y. Lv, Z. Song, L. Gan and M. Liu, *Mater. Horiz.*, 2025, **12**, 6733–6740.

27 W. Du, Q. Huang, Y. Lv, Z. Song, L. Gan and M. Liu, *Energy Environ. Sci.*, 2026, DOI: 10.1039/d5ee04802h.
28 Y. Zhang, F. Wan, S. Huang, S. Wang, Z. Niu and J. Chen, *Nat. Commun.*, 2020, **11**, 2199.
29 G. Zampardi and F. La Mantia, *Nat. Commun.*, 2022, **13**, 687.
30 J. J. Ye, P. H. Li, Z. Hou, W. Zhang, W. Zhu, S. Jin and H. Ji, *Angew. Chem., Int. Ed.*, 2024, **136**, e202410900.
31 M. Wu, Y. Sun, Z. Yang, S. Deng, H. Tong, X. Nie, Y. Su, J. Li and G. Chai, *Angew. Chem., Int. Ed.*, 2024, **136**, e202407439.
32 Q. He, T. Hu, Q. Wu, C. Wang, X. Han, Z. Chen, Y. Zhu, J. Chen, Y. Zhang, L. Shi, X. Wang, Y. Ma and J. Zhao, *Adv. Mater.*, 2024, **36**, 202400888.
33 Z. Song, W. Liu, Q. Huang, Y. Lv, L. Gan and M. Liu, *Chem. Sci.*, 2025, **16**, 16542–16551.
34 Y. Hu, P. Wang, M. Li, Z. Liu, S. Liang and G. Fang, *Energy Environ. Sci.*, 2024, **17**, 8078–8093.
35 Y. Qin, C. Hu, Q. Huang, Y. Lv, Z. Song, L. Gan and M. Liu, *Nano-Micro Lett.*, 2026, **18**, 38.
36 Y. Zhang, Z. Song, Q. Huang, Y. Lv, L. Gan and M. Liu, *Angew. Chem., Int. Ed.*, 2025, **64**, e202423936.
37 L. E. Blanc, D. Kundu and L. F. Nazar, *Joule*, 2020, **4**, 771–799.
38 S. Li, M. Li, X. Chi, X. Yin, Z. Luo and J. Yu, *Acta Phys. Chim. Sin.*, 2025, **41**, 100003.
39 D. Zhao, Q. Huang, Y. Lv, Z. Song, L. Gan and M. Liu, *Mater. Horiz.*, 2026, **13**, 252–261.
40 J. Yue, S. Chen, J. Yang, S. Li, G. Tan, R. Zhao, C. Wu and Y. Bai, *Adv. Mater.*, 2023, **36**, 202304040.
41 Y. Lu, Z. Wang, M. Li, Z. Li, X. Hu, Q. Xu, Y. Wang, H. Liu and Y. Wang, *Adv. Funct. Mater.*, 2024, **34**, 202310966.
42 P. Liu, Y. Lv, Z. Song, L. Gan and M. Liu, *Small*, 2025, DOI: 10.1002/smll.202511967.
43 L.-L. Zhao, Y.-H. Zhao, Y.-M. Wu, P.-F. Wang, Z.-L. Liu, Q.-Y. Zhang, J. Shu and T.-F. Yi, *Energy Storage Mater.*, 2025, **78**, 104299.
44 M. Yang, J. Zhu, J. Lin, L. He, M. Chen, Y. Wang, J. Chen, S. Zhong, H. Mi, C. He, D. Ma and P. Zhang, *Angew. Chem., Int. Ed.*, 2025, **64**, e202510893.
45 Y. Liu, Y. Sun, J. Zhang, X. Hao, M. Zhang, P. Wei, X. Zhao and K. Cai, *Nano Energy*, 2024, **120**, 109152.
46 Y. Zhang, Y. Fu, Y. Lv, Z. Song, L. Gan and M. Liu, *Chem. Commun.*, 2025, **61**, 14611–14624.
47 Y. Ding, C. Cai, L. Ma, J. Wang, M. P. Mercer, J. Liu, D. Kramer, X. Yu, D. Xue, C. Zhi and C. Peng, *Adv. Energy Mater.*, 2024, **15**, 2402819.
48 D. Zhang, Z. Song, Y. Chen, P. Liu, R. Gu, L. Miao, Y. Lv, Y. Wang, L. Gan and M. Liu, *Angew. Chem., Int. Ed.*, 2025, **64**, e21269.
49 F. Xiankai, X. Kaixiong, Z. Wei, D. Weina, Z. Hai, C. Liang and C. Han, *Carbon Energy*, 2024, **6**, e536.
50 X. Zhang, X. Ma, H. Bi, Y. Zhang, P. Mi, F. Liu, X. Jin, Y. Chen, K. Zhang, J. Wang and Y. Dong, *Adv. Funct. Mater.*, 2024, **35**, 2411990.
51 C. Wang, B. H. Xiao, J. Huang, K. Xiao and Z. Q. Liu, *Adv. Funct. Mater.*, 2024, **34**, 2405680.
52 X. Shi, C. Zhou, F. Yang, L. Shan, B. Tang, J. Zhang, Q. Nan, Y. Xie, J. Li, H. Li and X. Tian, *ACS Energy Lett.*, 2024, **9**, 1063–1072.
53 Q. Li, Q. Jiao, Z. Li, C. Lu, H. Yang, Y. Liu, Z. Yang and C. Feng, *Small*, 2024, **21**, 2409217.
54 Y.-Z. Zhu, K. Wang, S.-S. Zheng, H.-J. Wang, J.-C. Dong and J.-F. Li, *Acta Phys. Chim. Sin.*, 2024, **40**, 2304040.
55 M. Xie, X. Zhang, R. Wang, Y. Jiao, Z. Shu, S. Shan, Y. Bian, H. Lin, J. Chen and Y. Xu, *Chem. Eng. J.*, 2024, **494**, 152908.
56 C. Zhao, M. Wu, W. Lu, Y. Cheng, X. Zhang, I. Saadoune, R. Lian, Y. Wang and Y. Wei, *Small*, 2024, **20**, 202401379.
57 D. Qin, J. Ding, C. Liang, Q. Liu, L. Feng, Y. Luo, G. Hu, J. Luo and X. Liu, *Acta Phys. Chim. Sin.*, 2024, **40**, 2310034.
58 T. He, L. Xiao, J. Li and Y. Zhu, *J. Alloys Compd.*, 2025, **1015**, 178890.
59 Y. Wang, X. Wang, A. Zhang, X. Han, J. Yang, W. Chen, R. Zhao, C. Wu and Y. Bai, *Small*, 2024, **20**, 202403136.
60 Z. Zhou, J. Tong, X. Zou, Y. Wang, Y. Bai, Y. Yang, Y. Li, C. Wang and S. Liu, *J. Mater. Chem. A*, 2024, **12**, 10923–10931.
61 K. Zhu, W. Zhuang, N. Wang, K. Zhang, L. Lin, Z. Shao, C. Li, W. Wang, S. Liu, P. Yang, P. Xue, Q. Zhang, G. Hong and Y. Yao, *Adv. Mater.*, 2025, **37**, 2502366.
62 M. H. Alfaruqi, S. Islam, J. Gim, J. Song, S. Kim, D. T. Pham, J. Jo, Z. Xiu, V. Mathew and J. Kim, *Chem. Phys. Lett.*, 2016, **650**, 64–68.
63 O. Zhanadilov, H. J. Kim, A. Konarov, J. Jeong, J.-H. Park, K. Y. Chung, Z. Bakenov, H. Yashiro and S.-T. Myung, *Energy Storage Mater.*, 2024, **67**, 103283.
64 H. Ding, Y. He, X. Yu, L. Chen, M. Chen, Y. Luo, J. Li and S. Wei, *J. Electroanal. Chem.*, 2025, **986**, 119101.
65 W. Kao-ian, P. Tangthuam, P. Kidkhunthod, W. Limphirat, J. Padchasri, N. Aubert, G. Ciatto, I. In, K. C. W. Wu and S. Kheawhom, *Small Methods*, 2025, **9**, e00871.
66 R. Jin, Y. Fang, B. Gao, Y. Wan, Y. Zhou, G. Rui, W. Sun, P. Qiu and W. Luo, *Ind. Chem. Mater.*, 2025, **3**, 87–96.
67 A. Zhang, T. Chen, R. Zhao, Y. Wang, J. Yang, X. Han, X. Wang, C. Wu and Y. Bai, *Angew. Chem., Int. Ed.*, 2025, **64**, e202423824.
68 L. Wu, Z. Li, Y. Xiang, W. Dong, H. Wu, Y. Xu, Z. Ling, M. S. Chae, D. Sharon, N. Shpigel and X. Zhang, *ACS Energy Lett.*, 2024, **9**, 5801–5809.
69 J. Liang, Y. Zhao, L. Ren, M. Li, Q. Zhang, Y. Wang, X. Sun, M. Chuai, X. Wang and W. Liu, *Adv. Funct. Mater.*, 2025, **35**, 202501135.
70 Y. Chen, C. Lin, X. Chen, Z. Lu, K. Zhang, Y. Liu, J. Wang, G. Han and G. Xu, *Adv. Energy Mater.*, 2024, **14**, 202304303.
71 Y. Zhao, S. Zhang, Y. Zhang, J. Liang, L. Ren, H. J. Fan, W. Liu and X. Sun, *Energy Environ. Sci.*, 2024, **17**, 1279–1290.
72 H. Jia, Y. Li, U. Ali, B. Liu, Z. Jin, L. Li, Y. Chen, L. Zhang, T. Wang and C. Wang, *Nano Energy*, 2024, **122**, 109348.
73 Y. Huang, Y. Peng, Q. Ouyang, Q. Feng, H. Wang, D. Zheng, F. Wang, X. Lu and Q. Liu, *Energy Storage Mater.*, 2024, **70**, 103476.
74 J. Yang, X. Li, S. Wang, R. Liu, F. Zhang, G. Wang, J. Wang, W. Ren, J. Wu, K. Ji, Y. Ji, Z. Chen, B. J. Ni, Z. Yang, N. Wu and Y. M. Yan, *Adv. Funct. Mater.*, 2025, **36**, e13512.

75 H. Yang, Y. Wan, K. Sun, M. Zhang, C. Wang, Z. He, Q. Li, N. Wang, Y. Zhang, H. Hu and M. Wu, *Adv. Funct. Mater.*, 2023, **33**, 2215076.
76 Y. Fan, M. Xu, Q. Li, M. Liu, X. Zhang, P. Chu, B. Zhang, H. Zhou, Y. Zhao and C. Liu, *Small*, 2025, **21**, 202501454.
77 W. Lv, Z. Shen, X. Li, J. Meng, W. Yang, F. Ding, X. Ju, F. Ye, Y. Li, X. Lyu, M. Wang, Y. Tian and C. Xu, *Nano-Micro Lett.*, 2024, **16**, 109.
78 S. Jia, L. Li, Y. Shi, C. Wang, M. Cao, Y. Ji and D. Zhang, *Nanoscale*, 2024, **16**, 1539–1576.
79 J. Chacón-Borrero, X. Chang, Z. Min, J. Yu, G. Montaña-Mora, K. V. Mejia-Centeno, Y. Sun, X. Zhou, S. Tunmee, P. Kidkhunthod, J. Li, J. Llorca, J. Arbiol and A. Cabot, *Energy Storage Mater.*, 2025, **81**, 104486.
80 Y. Pan, S. Zuo, G. Ai, J. Wei, X. Zhao and W. Mao, *Small Methods*, 2024, **9**, 202401626.
81 X. Chen, Z. Xu, B. Sun, Q. Li, Q. Meng, F. Wei, J. Qi, Y. Sui and P. Cao, *J. Alloys Compd.*, 2025, **1020**, 179484.
82 Y. Liu, P. Shi, Y. Li, Y. Yang, J. Yao, J. Li, Z. Tao, Y. Gan, X. Liu, Z. Wu, C. Xia, J. Zheng, L. Lv, L. Tao, J. Zhang, H. Wang, H. Wan and H. Wang, *J. Energy Storage*, 2024, **96**, 112730.
83 S. Deng, B. Xu, X. Liu, Y. Yang, Y. Xiao, S. Wang, J. Zhao and T. Chen, *Adv. Funct. Mater.*, 2024, **35**, 202413711.
84 Y. Chen, L. Miao, Z. Song, H. Duan, Y. Lv, L. Gan and M. Liu, *Adv. Funct. Mater.*, 2024, **34**, 2409428.
85 T. Li, R. Guo, Y. Li, L. Meng, X. Sun, F. Li, X. Zhao, Z. Xu, J. Peng and L. An, *J. Energy Chem.*, 2023, **83**, 106–118.
86 R. Qin, S. Ding, C. Hou, L. Liu, Y. Wang, W. Zhao, L. Yao, Y. Shao, R. Zou, Q. Zhao, S. Li and F. Pan, *Adv. Energy Mater.*, 2023, **13**, 202203915.
87 Z. Shen, Y. Zhu, M. Zhang, T. Zhang, Z. Zhai, Y. Liu, L. Wang, Y. Wang, L. Li, G. Hong and N. Zhang, *ACS Energy Lett.*, 2025, **10**, 4491–4510.
88 X. Zeng, Z. Gong, C. Wang, P. J. Cullen and Z. Pei, *Adv. Energy Mater.*, 2024, **14**, 2401704.
89 Y. Liu, C. Lu, Y. Yang, W. Chen, F. Ye, H. Dong, Y. Wu, R. Ma and L. Hu, *Adv. Mater.*, 2024, **36**, 202312982.
90 J. Luo, M. Cao, N. Naresh, J. Borah, S. Li, T. Wang, B. K. Sarma, J. Yao, I. P. Parkin and B. D. Boruah, *Adv. Funct. Mater.*, 2024, **35**, 202417607.
91 J. Zhou, L. Shan, Z. Wu, X. Guo, G. Fang and S. Liang, *Chem. Commun.*, 2018, **54**, 4457–4460.
92 R. Sun, D. Luo, H. Zhou, Z. Zhang, Y. Gao, S. Ma, Z. Li and X. Kang, *J. Energy Chem.*, 2025, **103**, 703–713.
93 S. Deshmukh, J. V. Vaghasiya, J. Michalička, R. Langer, M. Otyepka and M. Pumera, *Small*, 2024, **21**, 202409987.
94 Y. Zhang, Z. Li, B. Zhao, D. Xu, Z. Guo, J. Zhang and C. Gong, *ACS Sustain. Chem. Eng.*, 2025, **13**, 2553–2563.
95 Y. Wang, Y. Fan, X. Chen, J. H. Liu, Y. Gao, X. Lin, Y. Huang, H. Jiang, C. Zhan, H. Zhang, X. Cao and Y. Xiao, *InfoMat*, 2025, e70055.
96 R. Sinha, X. Xie, Y. Yang, Y. Li, Y. Xue, P. Wang and Z. Li, *Adv. Energy Mater.*, 2025, **15**, 2404815.
97 B. Nie, S. Yu, K. Lu, H. Zhang, C. C. Yang and Q. Jiang, *Nano Lett.*, 2025, **25**, 10935–10943.
98 K. Guo, Z. Song, Y. Lv, L. Gan and M. Liu, *Adv. Funct. Mater.*, 2025, **35**, 202506036.
99 M. Zhu, R. Gao, Q. Ran, S. g. Gong, Q. Li, S. P. Zeng, H. Huang, L. Hu, D. Yang, T. Dai, Y. Wang, D. Chao, M. Feng and Z. Chen, *Angew. Chem., Int. Ed.*, 2025, **64**, e202425080.
100 M. Yang, Y. Lin, P. Chen, M. Lai, J. Zhu, G. Li, M. Chen, Y. Wang, M. Chuai, J. Chen, G. Chai, H. Mi, L. Sun, C. He, D. Ma and P. Zhang, *Angew. Chem., Int. Ed.*, 2025, **64**, e202510907.
101 D. Zhang, J. Cao, C. Yang, K. Lolupiman, W. Limphirat, X. Wu, X. Zhang, J. Qin and Y. Huang, *Adv. Energy Mater.*, 2024, **15**, 2404026.
102 Y. Liu, X. Wang, Z. S. Wu, Y. R. Cho and X. Wu, *Adv. Funct. Mater.*, 2025, **35**, 202505535.
103 P. Hu, T. Zhu, X. Wang, X. Wei, M. Yan, J. Li, W. Luo, W. Yang, W. Zhang, L. Zhou, Z. Zhou and L. Mai, *Nano Lett.*, 2018, **18**, 1758–1763.
104 P. Zhang, Y. Gong, S. Fan, Z. Luo, J. Hu, C. Peng, Q. Zhang, Y. Li and X. Ren, *Adv. Energy Mater.*, 2024, **14**, 2401493.
105 J. Xu, M. Galib, Z. Wu, L. Tao, Y. Shao, Y. Zhang, X. Guo, E. J. Hansen, Y. Chen, Z. Wang, C. Liu, M. Ponga and J. Liu, *Nano Energy*, 2024, **132**, 110373.
106 J. Liu, Z. Shen and C.-Z. Lu, *J. Mater. Chem. A*, 2024, **12**, 2647–2672.
107 H. Fu, X. Wang, L. Ye, Z. Wu, J. Yang, M. Shi and E. H. Ang, *Chem. Eng. J.*, 2025, **506**, 160308.
108 R. Trocoli and F. La Mantia, *ChemSusChem*, 2015, **8**, 481–485.
109 Y. Zeng, J. Xu, Y. Wang, S. Li, D. Luan and X. W. Lou, *Angew. Chem., Int. Ed.*, 2022, **61**, e202212031.
110 W. A. Syed, A. K. Kakarla, H. Bandi, R. Shanthappa and J. S. Yu, *J. Energy Storage*, 2024, **99**, 113325.
111 M. Zhang, W. Zhao, T. Yang, R. Gao, D. Luo, H. W. Park, Y. Hu and A. Yu, *Adv. Energy Mater.*, 2024, **14**, 202400543.
112 Y. Shi, B. Yang, G. Song, Z. Chen, M. Shakouri, W. Zhou, X. Zhang, G. Yuan and H. Pang, *Angew. Chem., Int. Ed.*, 2024, **63**, e202411579.
113 L. Wang, N. Liu, Q. Li, X. Wang, J. Liu, Y. Xu, Z. Luo, N. Zhang and F. Li, *Angew. Chem., Int. Ed.*, 2024, **64**, e202416392.
114 L. Zhou, C. Wu, F. Yu, Y. Li, H. Liu, C. Zheng, F. Shen, A. Wen and B. Wang, *ACS Appl. Mater. Interfaces*, 2024, **16**, 47454–47463.
115 M. Gu, A. M. Rao, J. Zhou and B. Lu, *Chem. Sci.*, 2024, **15**, 2323–2350.
116 M. Hariram, P. K. Pal, A. S. Chandran, M. R. Nair, M. Kumar, M. K. Ganesha, A. K. Singh, B. Dasgupta, S. Goel, T. Roy, P. W. Menezes and D. Sarkar, *Small*, 2025, **21**, 202410408.
117 X. Wen, Y. Zhong, S. Chen, Z. Yang, P. Dong, Y. Wang, L. Zhang, Z. Wang, Y. Jiang, G. Zhou, J. Liu and J. Gao, *Adv. Sci.*, 2024, **11**, 202309555.
118 H. Liang, Z. Cao, F. Ming, W. Zhang, D. H. Anjum, Y. Cui, L. Cavallo and H. N. Alshareef, *Nano Lett.*, 2019, **19**, 3199–3206.

119 Q. Liu, J. He, J. Xie, H. Zhang, H. Wu, G. Wang, X. Lu and Z. Yang, *Nano Energy*, 2024, **127**, 109780.
120 D. Jia, Z. Shen, W. Zhou, Y. Lv, Z. Chen, H. Tan, W. Zhou, X. He and H. Liu, *Chem. Eng. J.*, 2024, **500**, 156945.
121 S. Li, X. Zhao, T. Wang, J. Wu, X. Xu, P. Li, X. Ji, H. Hou, X. Qu, L. Jiao and Y. Liu, *Angew. Chem., Int. Ed.*, 2024, **63**, e202320075.
122 J. Xu, Z. Dong, Y. Li, K.-J. Huang, K. Liu and C. Cao, *Appl. Surf. Sci.*, 2023, **613**, 156146.
123 Z. H. Sun, W. Zheng, R. Zheng, Z. Y. Gu, Y. Bao, Z. B. Liu, Z. B. Sun, L. Niu and X. L. Wu, *Adv. Sci.*, 2025, **12**, e2502745.
124 Z. Yan, Q.-H. Yang and C. Yang, *J. Mater. Chem. A*, 2024, **12**, 24746–24760.
125 H. Zhao, L. Zhao, D. Yin, N. Gao, Y. Zhang, J. Feng, X. Chen, X. Liu, J. Wei, C. Fan, G. Gao, C. Xiao and S. Ding, *Adv. Mater.*, 2025, DOI: 10.1002/adma.202515759.
126 Y. Wu, Y. Qian, C. Huang, Y. Zhang, Y. Yang, A. Hu, Q. Tang and X. Chen, *Electrochim. Acta*, 2023, **460**, 142593.
127 M. Sun, L. Wei, J. Peng, G. Zhao, D. Yu and C. Chen, *J. Colloid Interface Sci.*, 2025, **698**, 138070.
128 Q. Zhang, H. Jiang, S. Liu, Q. Wang, J. Wang, Z. Zhou, K. Cai, Q. Lai and Q. Wang, *J. Power Sources*, 2024, **601**, 234286.
129 S. Zeng, S. Chen, Z. Ao, X. Lin, L. Yan, C. Liu and Z. Lin, *Small*, 2025, **21**, 2501695.
130 S. Chen, C. Peng, D. Zhu and C. Zhi, *Adv. Mater.*, 2024, **36**, 2409810.
131 L. Tang, C. Yuan, W. Lu and X. Li, *Adv. Funct. Mater.*, 2025, **35**, 2502455.
132 Y. Li, X. Guo, S. Wang, W. Sun, D. Yu, N. Li, H. Zhou, X. Zhang and H. Pang, *Adv. Sci.*, 2025, **12**, 2502563.
133 Y. Zhang, C. Wei, M.-X. Wu, Y. Wang, H. Jiang, G. Zhou, X. Tang and X. Liu, *Chem. Eng. J.*, 2023, **451**, 138915.
134 Y. Tulchinsky, C. H. Hendon, K. A. Lomachenko, E. Borfecchia, B. C. Melot, M. R. Hudson, J. D. Tarver, M. D. Korzyński, A. W. Stubbs, J. J. Kagan, C. Lamberti, C. M. Brown and M. Dincă, *J. Am. Chem. Soc.*, 2017, **139**, 5992–5997.
135 C. Dong, Y. Yu, C. Ma, C. Zhou, J. Wang, J. Gu, J. Ji, S. Yang, Z. Liu, X. Xu and L. Mai, *Energy Environ. Sci.*, 2025, **18**, 3014–3025.
136 N. Chen, W. Wang, Y. Ma, M. Chuai, X. Zheng, M. Wang, Y. Xu, Y. Yuan, J. Sun, K. Li, Y. Meng, C. Shen and W. Chen, *Small Methods*, 2023, **8**, 2201553.
137 T. Hu, Y. Zhao, Y. Yang, H. Lv, R. Zhong, F. Ding, F. Mo, H. Hu, C. Zhi and G. Liang, *Adv. Mater.*, 2024, **36**, 2312246.